

Control of a macro-micro actuated system

Kyoung Su Choi

MSc thesis



Control of a macro-micro actuated system

MASTER OF SCIENCE THESIS

For the degree of Master of Science in Mechanical Engineering at Delft
University of Technology

Kyoung Su Choi

24. 08. 2010

Faculty of Mechanical, Maritime and Materials Engineering (3mE) · Delft University of
Technology



Copyright © Delft Center for Systems and Control (DCSC)
All rights reserved.



Abstract

TU Delft Bio-Robotics Lab developed a new type of robotic arm, called a macro-micro actuated system for the inherent safety characteristics in human-interaction environment. The macro-micro actuated system is equipped with a macro actuator and a micro actuator which works together to control one joint angle. The macro actuator is connected to the link through a low stiffness spring, and the micro actuator is directly connected to the link. This was designed successfully to have the inherent safety of the robot arm. However, there remains the challenge of controlling the manipulator to possess the inherent safety with high-bandwidth performance and robustness, when the robot arm performs pick-and-place work of an unknown mass.

In this paper, first, the macro-micro actuated system of the Delft robot arm is introduced. Second, the control challenge to have safety with high-bandwidth performance is discussed along with possible control schemes for their successful implementation. Balancing/Tracking mode is chosen as the control scheme. In Balancing/Tracking mode, the macro actuator compensates for gravity and the micro actuator tracks the desired trajectory. Third, a feedback linearization method with a sliding mode algorithm and an indirect adaptive algorithm is surveyed to decrease nonlinearities of the system and to make the system robust. For fast estimation of an unknown variable and simplicity of a control algorithm, the sliding mode algorithm is applied to the chosen control scheme with the feedback linearization method. Finally, the Balancing/Tracking mode with the feedback linearization method and the sliding mode algorithm is proposed as the controller of the macro-micro actuated system.

Table of Contents

Preface	v
1 Introduction	1
1-1 Background	1
1-2 Delft robot arm	1
1-3 Problem definition	2
1-4 Assumption in control design	3
1-5 Organization	4
2 Modeling of a single link system	9
2-1 Description of the manipulator	11
2-2 Modeling of a manipulator	11
2-3 Modeling actuator dynamics	12
2-3-1 Hardware	12
2-3-2 A mathematical model	12
2-4 Overall dynamic model	14
2-5 Stability analysis of an open loop system	16
2-6 Conclusion	17
3 Analysis of control schemes	19
3-1 A simplified model of a single rotating link system	20
3-2 Control by only the macro actuator	20
3-3 Tracking/Compensating mode	28
3-4 Tracking/Tracking mode	29
3-5 Balancing/Tracking mode	30
3-6 Comparison of three control schemes	33
3-7 Conclusion	36

4	Controller	51
4-1	Feedback linearization control	51
4-2	Sliding mode control	58
4-3	Indirect adaptive control	65
4-4	Conclusion	69
5	Simulation with overall dynamic model	71
6	Conclusions and Recommendations	77
6-1	Conclusions	77
6-2	Recommendations	78
A	Stability Analysis	81
A-1	Problem Statement	81
A-2	Lyapunov direct method with Sector nonlinearity	82
A-2-1	The sector nonlinearity for a system assuming the system is in perfect static balance	83
A-2-2	The sector nonlinearity for a system assuming the mass is variable and observable	84
A-2-3	The sector nonlinearity for a system assuming the mass is variable, but unobservable	85
A-3	Vanishing Perturbation	85
B	PID cascade control	89
C	Cubic polynomial trajectory	93
D	Dynamics of a Delft robot arm	95
D-1	Kinematics	95
D-2	Dynamics	97
	Bibliography	99
	Glossary	101
	List of Acronyms	101
	List of Symbols	101

Preface

TU Delft Bio-Robotics Lab is developing the Delft robot arm. In this report, mathematical models are derived for the manipulator and the actuator of the Delft robot arm. Control schemes and controllers are designed to meet the requirements of the Delft robot arm.

The reader is assumed to have basic knowledge of mechanics and control theory. Some basic information on control and robotics is provided in Appendix A, B, C, and D. Readers who are interested in modeling a robot manipulator in Matlab/Simulink are referred in Chapter 2 and Appendix D. In these chapters, the modeling of the manipulator and the actuator is covered. Appendix A shows the stability analysis of a closed loop system, using the mathematical model. The control schemes with controllers of the manipulator can be found in Appendix B, Chapter 3 and 4. The simulation of overall dynamic model is represented in Chapter 5. A trajectory planner for the simulation is explained in Appendix C.

Acknowledgements.

I would like to thank my supervisor Prof. dr. Robert Babuška and Dr. ir. Martijn Wisse for their assistance during the writing of this thesis. Also I appreciate the help and support of Dr. ir. Zsofia Lendek.

Delft, University of Technology
24. 08. 2010

Kyoung Su Choi

“I may not be there yet, but I’m closer than I was yesterday.”

— *Author Unknown*

Chapter 1

Introduction

1-1 Background

Many robot arms such as farm robots, medical robots, and service robots have been developed to provide both safety and high-bandwidth performance in human-interaction environment [1]. In conventional highly geared robot arms, an actuator and a link are stiffly connected, giving conventional robot arms high bandwidth. However, they are not safe since the high power of actuator transfers to the contact environment or the human without any compliance. To improve the safety of a robot arm, Series Elastic Actuation (SEA) robot arms were developed [2]. A SEA robot arm consists of a low stiffness spring between the actuator and the link. The spring increases the safety of the robot arm by decreasing the contact force in the case of an unexpected impact, but it also results in a bandwidth limitation of the robot arm. In addition, attenuation of flexible mode oscillation excited by disturbances can be difficult to achieve [3].

To overcome the drawbacks of the series elastic actuation method, macro-micro actuated robot arms were developed [1]. These robots are equipped with two actuators, a macro actuator and a micro actuator, which work together to control one joint angle or one axis motion. The macro actuator is connected to the link through a low stiffness spring similarly to the actuator of SEA robot arms, and the micro actuator is directly connected to the link with a gear-box. TU Delft Bio-Robotics Lab has developed the macro-micro actuated robot arm, called the Delft robot arm [4, 5]. Its main function is pick-and-place work with an unknown mass held by the end-effector as shown in Figure 1.1. When the robot arm moves point to point with an unknown mass, it has to be both fast and accurate with low actuating power for both safety and high-bandwidth performance.

1-2 Delft robot arm

The Delft robot arm is shown in Figure 1.2. The arm has four Degrees of Freedom (DOF) with four rotation joints ($\varphi_1, \varphi_2, \varphi_3, \varphi_4$), and two translation joints (a_2, a_4). The four rotation

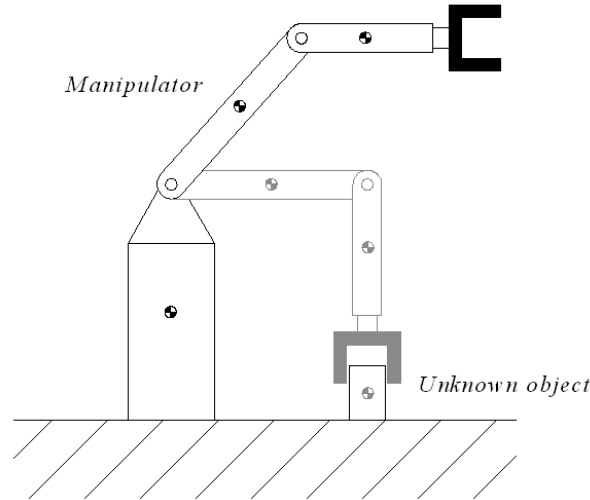


Figure 1-1: An example task of a Delft robot arm; pick-and-place motions with objects of an unknown mass

joints (φ_i) are actuated by four motors with gearbox, which are called as micro actuators. The translation joints (a_i) are connected to the joint φ_2 and φ_4 through springs respectively, and those are actuated by two motors with a lead screw, which are called macro actuators.

Figure 1.3 shows a schematic diagram of the robot kinematics. It consists of the three major links (L_{12}, L_{34}, L_{m4}) attached to the four rotation joints ($\varphi_1, \varphi_2, \varphi_3, \varphi_4$), and the three minor links (L_{ab}, L_{b3}, L_{a4}) with the two passive joints (φ_a, φ_b). The two translation joints (a_2, a_4), which are not expressed in this figure, are connected to L_{34} and L_{m4} by wire and spring. Thus, the joint angles, φ_2 and φ_4 , are driven by one macro actuator and one micro actuator. Joint angles, φ_1 and φ_3 , are driven by single actuators. The passive joints, φ_a and φ_b , follow joint angle φ_4 and φ_2 respectively.

In the macro-micro actuated systems of joint angle φ_2 and φ_4 , micro actuators control the joint angles directly, and macro actuators control the joint angles indirectly via springs as shown in Figure 1.4. In this project, the macro-micro actuated system for one joint angle in Figure 1.4 is considered for the positioning task with an unknown mass. The two actuators should cooperate to obtain maximal performance, while the safety is guaranteed because of the special construction with springs in the macro actuation.

1-3 Problem definition

The goal of this report is to find the best control scheme with a controller for the macro-micro actuated system. To reach this goal, four subgoals are formulated. In Section 6.1, the conclusions are drawn based on the four subgoals.

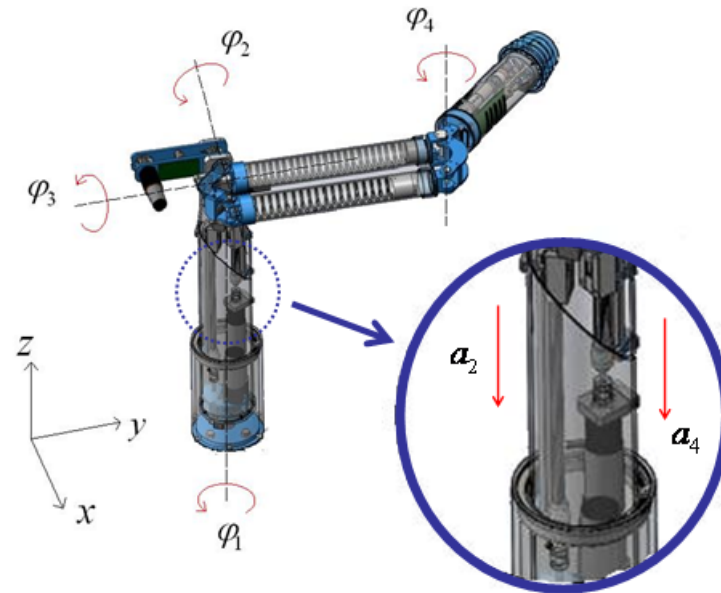


Figure 1-2: The Delft robot arm developed at the Delft Bio-Robotics Lab.

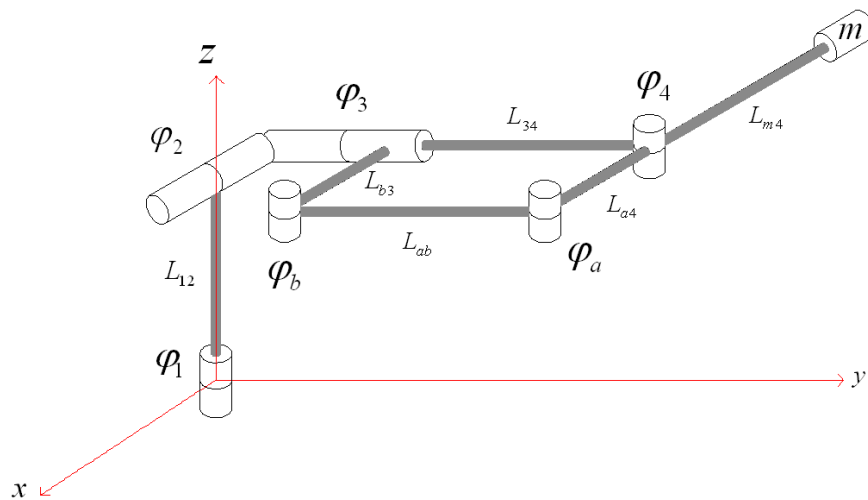


Figure 1-3: A schematic diagram of the robot kinematics; the diagram shows the parallel mechanism which allows the application of macro-micro actuation for both the shoulder and elbow joint.

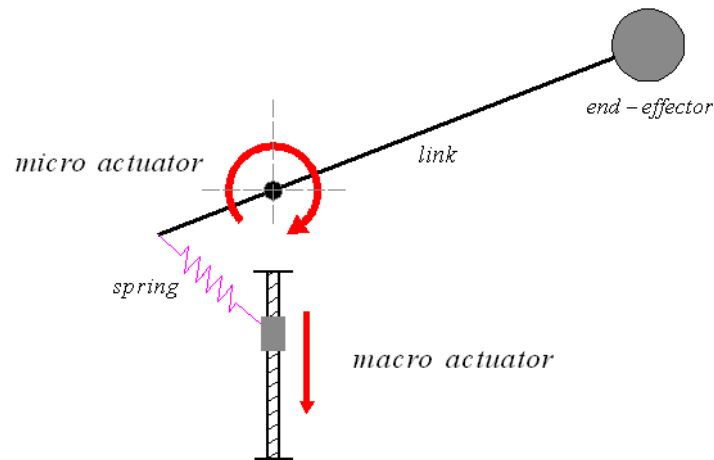


Figure 1-4: A schematic diagram of a simplified model, one-DOF macro-micro actuated system; this report focuses on this simplified model

1. In order to simulate the manipulator, a dynamic model of the manipulator and actuator dynamics are required. This dynamic model must include the following characteristics: inertia, gravitational forces, and Coriolis and centrifugal forces. A visual representation is needed to understand the motion and the dynamic model.
2. To analyze the system properties, it is required to check the nonlinearity of the system, the influence of an unknown mass attached to the end-effector, the stability of the Multi-Input-Multi-Output (MIMO) system, and the performance limitations by the kinematic limits and actuation saturations.
3. The third subgoal is to survey several control schemes. The control schemes must have adaptivity or robustness against the mass variation of the end-effector, which should be represented by design methods such as root locus.
4. To choose the best control scheme for the macro-micro actuated system, the performance of the system with the control schemes and controllers have to be compared. The system must have low actuation power of the micro actuator, less than 0.5 degree position error and high-bandwidth performance in the given ranges of motor speeds, motor torques, current, and voltage.

1-4 Assumption in control design

The following assumption are made for modeling the single rotating link system in Figure 1.4.

- There are two DOF, one rotational joint and one translational joint.
- The operational angle of the link is between 30 and 150 degrees.
- The lead screw length is from -0.01m to -0.25m, originated from the rotation point of the link.

- The mass variation of the end-effector including the load is between 0.35kg and 2kg.
- The mass of the link is neglected, only the mass of the end-effector is considered.
- The inertia of the gear and lead screw is neglected.
- The spring is ideal. 'Ideal' means the spring is linear.
- There is no friction in the system such as static friction, coulomb friction and viscous friction; the gear efficiency is 100%. Only viscous damping of motors is considered.
- Voltage control is considered.
- The Performance specification for controller design are 0.5 degrees tracking error, 1.5 sec. settling time, and less than 5% overshoot. 0.5 degrees error means that the end-effector position is apart by 3mm from the desired position. A settling time of 1.5 sec. is an average time to have one movement of human to pick or place an unknown mass [4]. These are acceptable specification for farm robots and service robots which do not need high precision works.

The parameters and actuator dynamics are based on the actuating system of the joint angle φ_4 of the Delft robot arm. The parameter values are mentioned in Table 5-1 and 5-2 of Chapter 5.

1-5 Organization

The contents of this report is organized in six chapters; Figure 1.5 shows a flow chart of global strategy to solve the problems in Section 1.3. In Chapter 2, the single rotating link system is described, and mathematical models of the manipulator and actuator dynamics are derived. The stability of an open loop system is also analyzed. Chapter 3 compares three control schemes: Tracking/Compensating mode, Tracking/Tracking mode, and Balancing/Tracking mode. A control scheme which has the smallest torque of the micro actuator is chosen as the best scheme, when the three control schemes have same performance. Chapter 4 shows a feedback linearization method to decrease nonlinearities of the system, based on the chosen control schemes in Chapter 3 . Two advanced algorithms, a sliding mode algorithm and an indirect adaptive algorithm, are applied to the feedback linearization method for robustness of the system. One of the advanced algorithm which has faster estimation is selected for a final controller. In Chapter 5, the overall dynamic model of the single rotating link system is simulated with the chosen controller considering various saturations and limitations of the system. Finally, the conclusions are given in Chapter 6, followed by the recommendations.

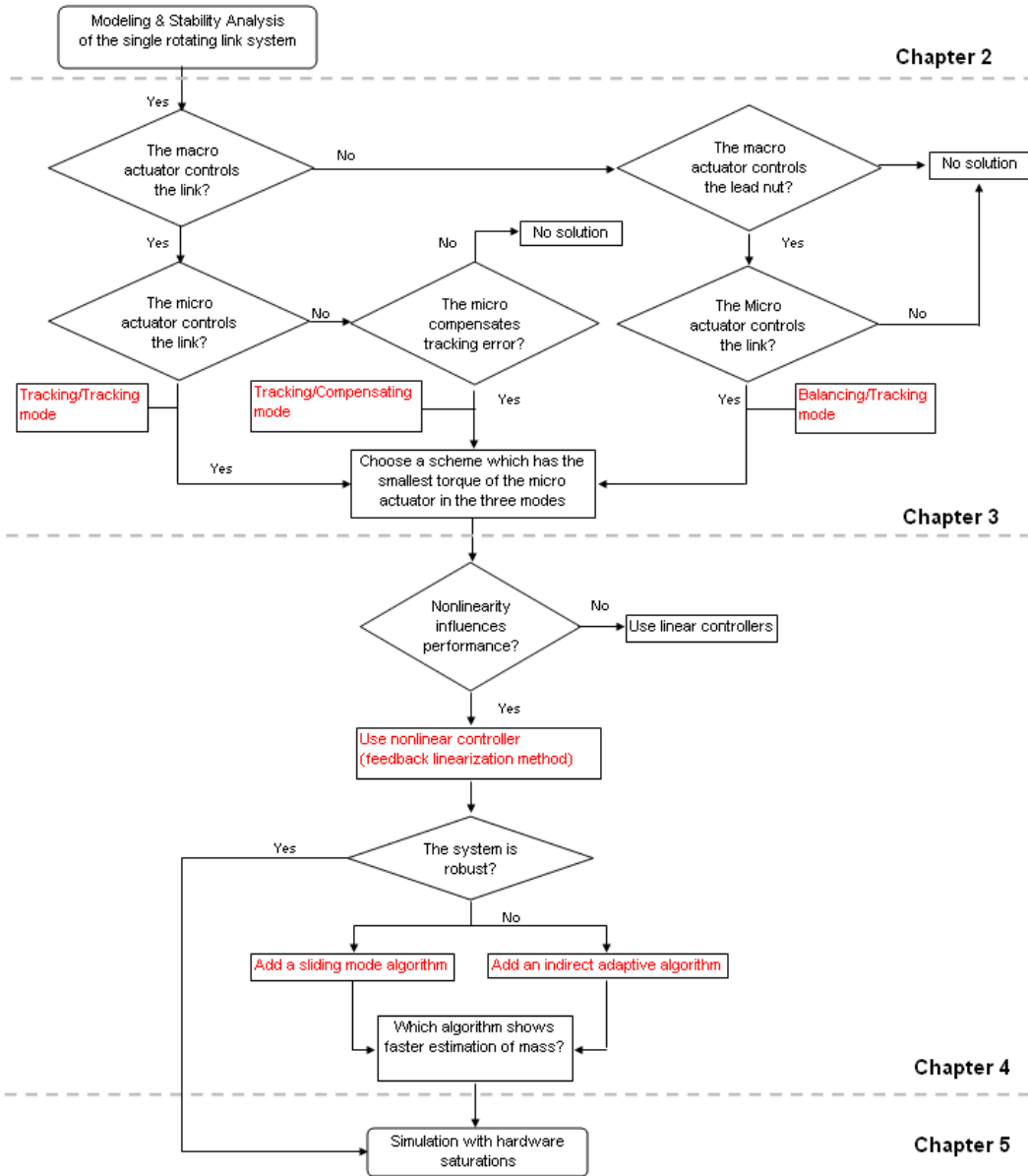


Figure 1-5: A flow chart of global solution strategy

Chapter 2

Modeling of a single link system

The first step in this project is to develop a mathematical model of the single rotating link system, which has macro-micro actuation. This model can be used to simulate the dynamic behavior of the single rotating link system. Additionally, the dynamic behavior includes the interaction of the macro-micro actuators. The model can also be used to analyze the stability of the system and to find a proper control scheme. Control schemes can be tested on the model before implementing them on an extended model including actuator dynamics.

The model of the single rotating link system is depicted in Figure 2.1. It is modeled as two separated parts; a model of the manipulator and a model of the actuator dynamics. The manipulator dynamics are described in free space. This model takes into account inertia properties, viscous damping of actuators, and gravitational torques. The model of the actuator dynamics describes the behavior with electrical factors, such as inductance and resistance, and kinematic factors such as gear ratios and the pitch of the lead screw. The two models are combined to represent the system as in whole.

This chapter is organized as follows: In Section 2.1, the single rotating link system is described. In Section 2.2, the dynamic model of the manipulator of the single rotating link system in free space is calculated. In Section 2.3, mathematical models of the actuator dynamics are derived and the hardware properties of the actuator dynamics are introduced. In Section 2.4, an overall dynamic model is derived, consisting of the combined mathematical models of the manipulator and the actuator dynamics. Finally, the stability of the open loop system of the overall dynamic model is analyzed.

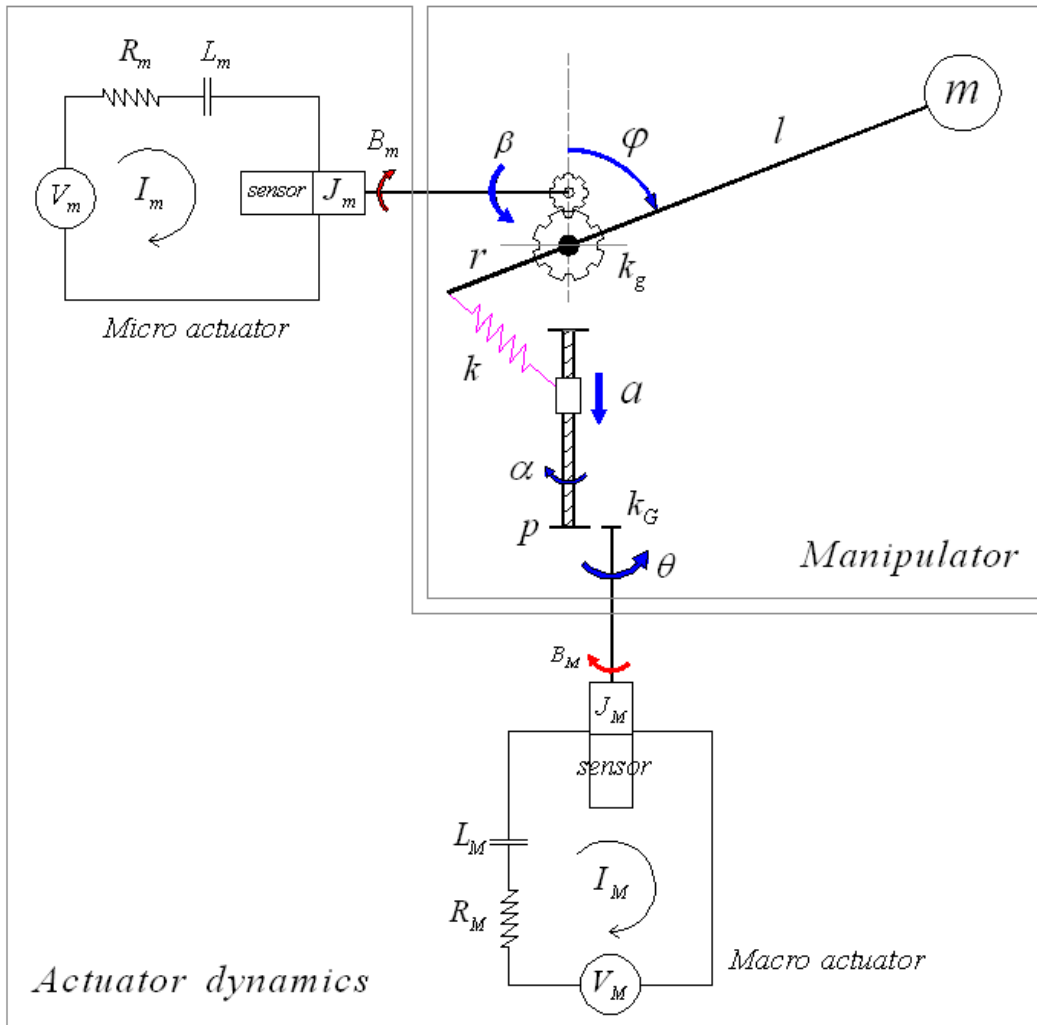


Figure 2-1: Diagram of the single rotating link system

k	spring coefficient	φ	angle of the link
r	link length	l	link length
m	mass of the end-effector	α	angle of the lead screw
a	distance of the lead nut	p	pitch of the lead screw
β	angle of the micro actuator	θ	angle of the macro actuator
J_m	rotor inertia of the micro actuator	J_M	rotor inertia of the macro actuator
L_m	inductance of the micro actuator	L_M	inductance of the macro actuator
R_m	resistor of the micro actuator	R_M	resistor of the macro actuator
V_m	voltage of the micro actuator	V_M	voltage of the macro actuator
I_m	current of the micro actuator	I_M	current of the macro actuator
B_m	viscous damping of the micro actuator	B_M	viscous damping of the macro actuator
k_g	gear ratio of the micro actuator	k_G	gear ratio of the macro actuator

Table 2-1: Definition of parameters

2-1 Description of the manipulator

The single rotating link system, which is a simplified version of joint angle φ_4 of the Delft Robot Arm, is shown in Figure 2.1. It consists of the actuator and the manipulator dynamics. The manipulator is controlled by macro-micro actuators. These are connected to the manipulator in parallel. The macro actuator is driven by current (I_M) generated by voltage (V_M) and an electrical circuit. Its rotation (θ) transfers a reduced rotation (α) with an increased torque by a gearbox (k_G) to a lead screw, and the lead screw changes the rotation to translation (a) through a leadscrew nut. The motion of the leadscrew nut rotates the link through a spring (k). The micro actuator is driven by current (I_m) generated by voltage (V_m) and an electrical circuit. The rotation (β) transfers a reduced rotation (φ) with an increased torque to the link through a gearbox (k_g). The mass of an end-effector of the link is changed since an end-effector of the Delft robot arm does pick-and-place work of an unknown mass.

2-2 Modeling of a manipulator

In this section, the mathematical model of the manipulator of the single rotating link system in Figure 2.1 is derived using the Lagrangian method. The kinetic energy, T , and the potential energy, V , with two inputs, τ_M and τ_m , are expressed as follows.

$$\frac{d}{dt}\left(\frac{\partial T}{\partial \dot{q}_j}\right) - \frac{\partial T}{\partial q_j} + \frac{\partial V}{\partial q_j} = \tau_j$$

$$T = \frac{1}{2}J\dot{\varphi}^2 = \frac{1}{2}ml^2\dot{\varphi}^2 = \frac{1}{2}ml^2\left(\frac{\dot{\beta}}{k_g}\right)^2$$

$$\begin{aligned} V &= \frac{1}{2}k[\sqrt{(-r \sin \varphi)^2 + (-r \cos \varphi + a)^2}]^2 + mgl \cos \varphi \\ &= \frac{1}{2}k(r^2 + a^2 - 2ar \cos \varphi) + mgl \cos \varphi \\ &= \frac{1}{2}k\left(r^2 + \left(\frac{n\theta}{k_G}\right)^2 - \frac{2nr\theta}{k_G} \cos \frac{\beta}{k_g}\right) + mgl \cos \frac{\beta}{k_g} \end{aligned}$$

where $q = [\beta, \theta]$, $\tau = [\tau_m, \tau_M]$, $\varphi = \frac{\beta}{k_g}$, $a = n\alpha = \frac{n\theta}{k_G}$, and $n = \frac{p}{2\pi}$

The resulting equations of the motion of the system are

$$\begin{cases} \frac{ml^2}{k_g^2}\ddot{\beta} + \frac{1}{k_g}\left(\frac{knr\theta}{k_G} - mgl\right) \sin \frac{\beta}{k_g} = \tau_m \\ \frac{kn^2\theta}{k_G^2} - \frac{knr}{k_G} \cos \frac{\beta}{k_g} = \tau_M \end{cases} \quad (2-1)$$

The first motion equation is for the micro part, and the second motion equation is for the macro part.

2-3 Modeling actuator dynamics

The actuator dynamics have to be considered to simulate the overall dynamics model. The inertia of the rotor influences the motion of the system, and the actuators have various saturations and limitations such as current saturation, voltage saturation, maximum motor speed, and maximum motor torque, which limit the performance of the system. First, the properties of hardware are introduced, and then the mathematical model of the actuator dynamics is derived.

2-3-1 Hardware

Actuators

The micro actuator is Maxon DC motor No. 110164, and its maximum angular speed and maximum torque are 1026 rad/s and 0.00697 Nm. The macro actuator is Maxon DC motor No. 323890, and its maximum angular speed and maximum torque are 1256 rad/s and 0.0933 Nm. Viscous dampings of both motors are 5.8×10^{-6} (kgm^2/sec).

Amplifiers

The motor driver of the Delft robot arm is Acroname No.S11-3A-EMF-H-BRIDGE. The amplifier is set up for voltage control with maximum motor voltage of 27.5V, maximum continuous current of 3A, and maximum surge current of 6A for a duration of 0.2sec.

Sensors

An encoder is placed at the motor part, not the link part so that the motor angle is fed back and the angular velocity of the motor is measured by a back EMF measurement circuit in the amplifier module. The encoder of the micro actuator is Maxon No. 225805, and the encoder of the macro actuator is Maxon No. 201937. Both sensitivities are 512 counts per turn (cpt).

2-3-2 A mathematical model

The actuator dynamics of the two actuators of the single rotating link system are shown in Figure 2.1, and the parameters of the actuator dynamics are defined in Table 2.2. The kinetic energy and dissipation energy, T and D of the micro actuator are:

$$T = \frac{1}{2}J_m\dot{\beta}^2 + \frac{1}{2}L_m I_m^2$$

$$D = \frac{1}{2}B_m\dot{\beta}^2 + \frac{1}{2}R_m I_m^2$$

Using the above energy equations and the Lagrangian, motion equations of the actuator are derived:

$$J_m\ddot{\beta} + B_m\dot{\beta} + T_l = T_m$$

$$L_m\dot{I}_m + R_m I_m = V_m - V_b$$

Using Laplace transformation, the above motion equations are written in below equations and expressed in a block diagram of Figure 2.2.

$$\begin{cases} \beta(s) = \frac{1}{s} \frac{T_m - T_l}{J_m s + B_m} = \frac{1}{s} \left(\frac{k_i I_m(s)}{J_m s + B_m} - \frac{T_l}{J_m s + B_m} \right) \\ I_m(s) = \frac{V_m}{L_m s + R_m} - \frac{V_b}{L_m s + R_m} = \frac{1}{L_m s + R_m} (V_m - s k_b \beta(s)) \end{cases} \quad (2-2)$$

where $T_m = k_i I_m$ and $V_b = k_b \dot{\beta}$

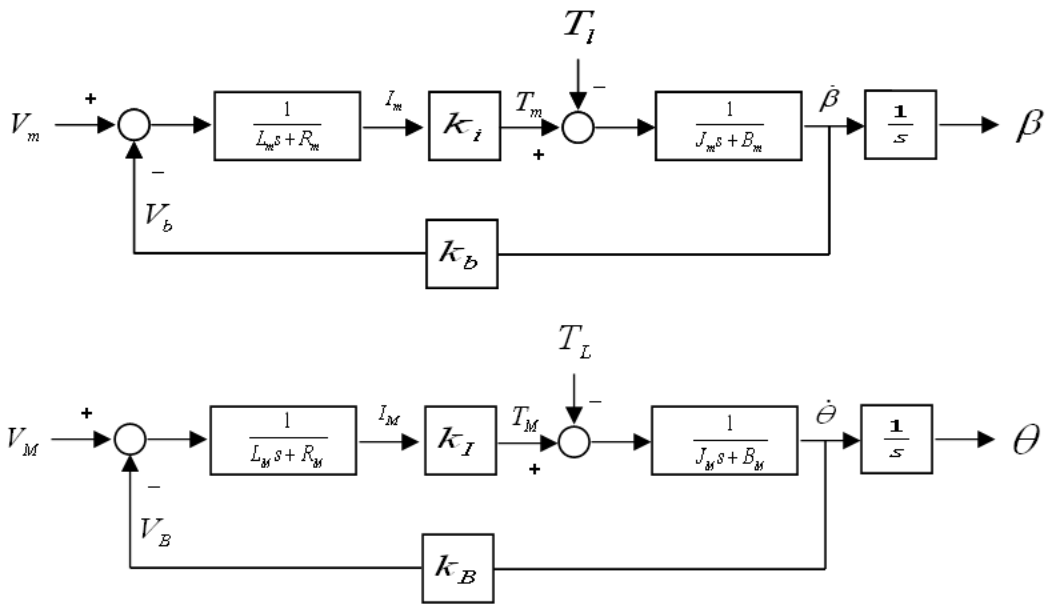


Figure 2-2: Block diagrams of the actuator dynamics of the micro actuator (top figure) and the macro actuator (bottom figure)

V_m	Voltage of the micro actuator	V_M	Voltage of the macro actuator
R_m	Resistance of the micro actuator	R_M	Resistance of the macro actuator
L_m	Inductance of the micro actuator	L_M	Inductance of the macro actuator
T_l	Load torque of the micro actuator	T_L	Load torque of the macro actuator
T_m	Motor torque of the micro actuator	T_M	Motor torque of the macro actuator
V_b	Back emf Voltage of the micro actuator	V_B	Back emf Voltage of the macro actuator
J_m	Rotor inertia of the micro actuator	J_M	Rotor inertia of the macro actuator
k_b	Back emf constant of the micro actuator	k_B	Back emf constant of the macro actuator
B_m	Viscous damping of the micro actuator	B_M	Viscous damping of the macro actuator
k_i	Torque constant of the micro actuator	k_I	Torque constant of the macro actuator
β	Motor angle of the micro actuator	θ	Motor angle of the macro actuator

Table 2-2: Parameters of actuator dynamics

The kinetic energy and dissipation energy, T and D of the macro actuator are:

$$T = \frac{1}{2}J_M\dot{\theta}^2 + \frac{1}{2}L_M I_M^2$$

$$D = \frac{1}{2}B_M\dot{\theta}^2 + \frac{1}{2}R_M I_M^2$$

Using the above energy equations, motion equations of the actuator are derived:

$$J_M\ddot{\theta} + B_M\dot{\theta} + T_L = T_M$$

$$L_M\dot{I}_M + R_M I_M = V_M - V_B$$

Using Laplace transformation, the above motion equations are written in below equations and expressed in the block diagram of Figure 2.2.

$$\begin{cases} \theta(s) = \frac{1}{s} \frac{T_M - T_L}{J_M s + B_M} = \frac{1}{s} \left(\frac{k_I I_M(s)}{J_M s + B_M} - \frac{T_L}{J_M s + B_M} \right) \\ I_M(s) = \frac{V_M}{L_M s + R_M} - \frac{s k_B \theta(s)}{L_M s + R_M} = \frac{1}{L_M s + R_M} (V_M - s k_B \theta(s)) \end{cases} \quad (2-3)$$

where $T_M = k_I I_M$ and $V_B = k_B \dot{\theta}$

2-4 Overall dynamic model

The mathematical model of the actuator dynamics and the manipulator are combined as shown in Figure 2.1. The combined model is used to choose proper gains of the system considering the link limitation, maximum motor speeds, maximum motor torques, current saturations and voltage saturations of the macro-micro actuators in Chapter 5.

Two second order Differential Algebraic Equations (DAEs) are derived using equation 2-1, 2-2, and 2-3 with assumption of $L_m = L_M = 0$, since the inductances are very small values. The first equation is the motion equation of the micro actuator, and the second equation is the motion equation of the macro actuator; where $\beta = k_g \varphi$, $T_l = \frac{T}{k_g}$, $\theta = k_G \alpha$, and $T_L = \frac{T_\alpha}{k_G} = \frac{nF}{k_G}$.

$$\begin{cases} \frac{R_m}{k_i} (J_m + \frac{ml^2}{k_g^2}) \ddot{\beta} + (\frac{R_m B_m}{k_i} + k_b) \dot{\beta} + \frac{R_m}{k_i k_g} (\frac{knr\theta}{k_G} - mgl) \sin \frac{\beta}{k_g} = V_m \\ \frac{R_M J_M}{k_I} \ddot{\theta} + (\frac{R_M B_M}{k_I} + k_B) \dot{\theta} + \frac{R_M}{k_I k_G} (\frac{kn^2\theta}{k_G} - knr \cos \frac{\beta}{k_g}) = V_M \end{cases} \quad (2-4)$$

2-5 Stability analysis of an open loop system

Before analyzing the closed loop behavior in Chapter 3, first the open loop behavior of the single rotating link system as an autonomous system is analyzed using the Lyapunov method. Only the first equation of equation 2-4 is considered to know the stability and motion of the single rotating link depending on the distance a . The motion equation can be expressed in variables of φ and a to understand the system easily:

$$\frac{R_m}{k_i}(J_m k_g^2 + ml^2)\ddot{\varphi} + k_g^2\left(\frac{R_m B_m}{k_i} + k_b\right)\dot{\varphi} + \frac{R_m}{k_i k_g}(kar - mgl)\sin\varphi = V_m$$

This nonlinear equation has infinite equilibrium points, and those are categorized in three sets, $q_{eq}=(\varphi_e, a_e)=(0, \infty), (\pi, \infty), (\infty, \frac{mgl}{kr})$. These three equilibrium point sets show that any distance a is an equilibrium point when $\varphi=0$ and π , and all angles are equilibrium points of the system when $a = \frac{mgl}{kr}$. Linearized motion equations of the above motion equation with the three equilibrium point sets are

$$\left\{ \begin{array}{l} \text{when } q_{eq} = (0, a_e), \quad \frac{R_m}{k_i}(J_m k_g^2 + ml^2)\ddot{\varphi} + k_g\left(\frac{R_m B_m}{k_i} + k_b\right)\dot{\varphi} + \frac{R_m}{k_i k_g}(ka_e r - mgl)\sin\varphi = V_m \\ \text{when } q_{eq} = (\pi, a_e), \quad \frac{R_m}{k_i}(J_m k_g^2 + ml^2)\ddot{\varphi} + k_g\left(\frac{R_m B_m}{k_i} + k_b\right)\dot{\varphi} + \frac{R_m}{k_i k_g}(-ka_e r + mgl)\sin\varphi = V_m \\ \text{when } q_{eq} = (\varphi_e, \frac{mgl}{kr}), \quad \frac{R_m}{k_i}(J_m k_g^2 + ml^2)\ddot{\varphi} + k_g\left(\frac{R_m B_m}{k_i} + k_b\right)\dot{\varphi} + \frac{R_m}{k_i k_g}kar\sin\varphi_e = V_m \end{array} \right.$$

Three motion rules are derived from the above linearized equations and Lyapunov first method.

1. When $a_e > \frac{mgl}{kr}$, the link converges to 0 degrees (asymptotically stable) since the two eigenvalues of the first linearized equation are placed in the left half plane (LHP) in frequency domain.
2. When $a_e < \frac{mgl}{kr}$, the link converges to 180 degrees (asymptotically stable) since the two eigenvalues of the second linearized equation are placed in the LHP in frequency domain.
3. When $a = \frac{mgl}{kr}$, the link keeps its initial angle while torque is not applied (marginally stable) since one eigenvalue of the third linearized equation is placed at origin; the other eigenvalue is in the LHP.

These can be confirmed by an open loop simulation of the original nonlinear system as shown in Figure 2.3. From the first and second graph, the link converges to 0 and 180 degrees asymptotically when $a > \frac{mgl}{kr}$ and $a < \frac{mgl}{kr}$. On the other hands, according to the third graph, the link is in static balance even though the initial angle is changed, only if the leadscrew nut is placed at $a = \frac{mgl}{kr}$. That is, when the macro actuator locates the lead nut at the static balancing point, $\frac{mgl}{kr}$, the micro actuator does not need to provide torque to compensate for gravity, since the gravity torques factor of the motion equation is removed. The link has motion while the micro actuator generates torque. This static balancing concept is used in control schemes of Chapter 3.

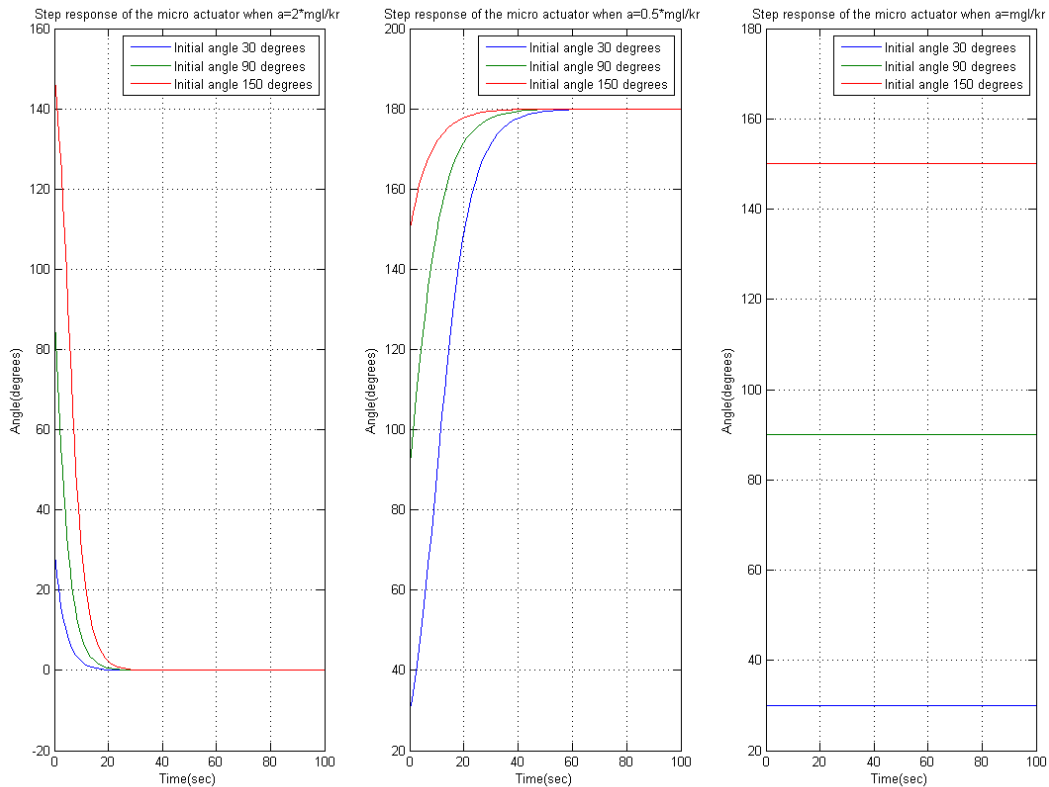


Figure 2-3: Variation of angle φ at initial angle 45, 90, and 135 degrees

2-6 Conclusion

This chapter showed the modeling of the single rotating link system to design control schemes in next chapter. Motion equations of the manipulator and the actuator dynamics were derived using the Lagrange method. The original nonlinear model was linearized to check the stability of the open loop system around the operating point. When the system is in static balance ($a = \frac{mgl}{kr}$), the link keeps its initial state, as long as an external torque is not applied. As a result, the system is marginally stable in static balance. On the other hand, when the system is not in static balance ($a \neq \frac{mgl}{kr}$), the link converges to 0 or 180 degrees. This static balancing concept is used to design control schemes since it makes that the micro actuator does not need to provide torque to compensate for gravity.

Chapter 3

Analysis of control schemes

In this chapter, the three candidate control schemes for the single rotating link system are researched and compared through simulation. For a fast calculation, a simplified model of the single rotating link system is employed instead of the overall dynamic model in this chapter. The simplified model in Section 3.1 is to design the control schemes with stability analysis of a closed loop system. Next, it is shown in Section 3.2 whether the macro actuator can control the link or not and whether linear controllers based on a linearized system model can be used or not. And then, three control schemes are surveyed, namely Tracking/Compensating mode, Tracking/Tracking mode, and Balancing/Tracking mode. These control schemes give different roles to macro/micro actuators as shown in Table 3.1. The three control schemes are analyzed in Section 3.3, 3.4, and 3.5. Finally, the three control schemes are compared in Section 3.6.

Roles	Tracking /Compensating mode	Tracking /Tracking mode	Balancing /Tracking mode
Static balance	M		M
Trajectory tracking	M	M, m	m
Compensating tracking error of the macro actuator	m		

Table 3-1: Roles of three control schemes(M: Macro actuator, m: Micro actuator)

3-1 A simplified model of a single rotating link system

A simplified model of the single rotating link system neglects actuator dynamics and gear ratio as shown in Figure 3.1. Then, the motion equations of the simplified model are represented as follows; the parameter values of Table 3.2 is substituted for time responses and frequency responses.

$$\begin{cases} ml^2\ddot{\varphi} + (kar - mgl) \sin \varphi = \tau \\ ka - kr \cos \varphi = F \end{cases} \quad (3-1)$$

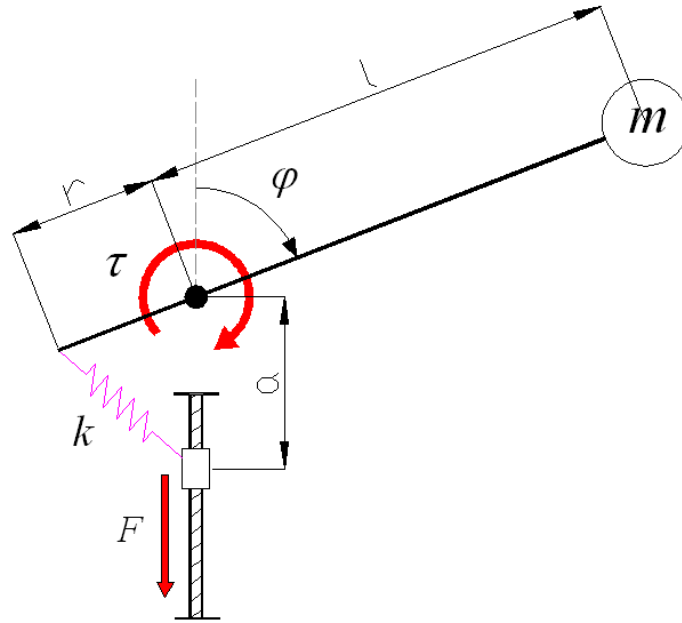


Figure 3-1: Diagram of the simplified model of the single rotating link system

g	9.8 [kgm/s ²]	m	0.35 [kg]
r	0.075 [m]	l	0.4 [m]
n	1 [-]	k	568 [kg/s ²]
k_G	1 [-]	k_g	1 [-]

Table 3-2: Parameters for the simplified model of the single rotating link system

3-2 Control by only the macro actuator

For the first step, the characteristics of the macro actuator are surveyed by neglecting the micro actuator. It is assumed that τ equals zero and the distance a is used as the control input to control angle φ in equation 3-1. Then, the equation 3-1 is expressed as one equation:

$$ml^2\ddot{\varphi} + (kar - mgl) \sin \varphi = 0$$

Linearizing the above motion equation using an equilibrium point $(\infty, \frac{mgl}{kr})$ because the other equilibrium sets are meaningless for trajectory tracking,

$$ml^2\ddot{\varphi} + kar \sin \varphi_e = 0$$

The transfer function $\frac{\varphi(s)}{a(s)}$ is expressed as follows.

$$G(s) = \frac{\varphi(s)}{a(s)} = \frac{-kr \sin \varphi_e}{ml^2 s^2}$$

A PD controller is considered to control this system. The closed loop system is expressed as the following Laplace form; where φ_d is a desired angle, k_p is a proportional gain, and k_d is a differential gain.

$$ml^2\varphi(s)s^2 + kr \sin \varphi_e a(s) = 0 \quad \text{where} \quad a = -k_d\varphi(s)s + k_p(\varphi_d - \varphi(s))$$

Then, the transfer function of the closed loop system is

$$\frac{\varphi(s)}{\varphi_d(s)} = \frac{-k_p kr \sin \varphi_e}{ml^2 s^2 - k_d kr \sin \varphi_e s - k_p kr \sin \varphi_e} = \frac{-k_p z}{s^2 - k_d z s - k_p z} \quad \text{where} \quad z = \frac{kr \sin \varphi_e}{ml^2}$$

Using the transfer function, the conditions for the gains of controller are derived which make the closed loop system stable.

$$\begin{cases} \text{when } 0 < \varphi_e < 180, & k_d < 0, k_p < 0 \\ \text{when } -180 < \varphi_e < 0, & k_d > 0, k_p > 0 \end{cases} \quad (3-2)$$

In this project, since the operating range of the link is between 30 degree and 150 degree, the gains have to be smaller than zero from the above rules. The gains of the PD controller are chosen by Root Locus method assuming the ratio of the differential gain and the proportional gain, $\frac{k_d}{k_p}$, as 0.3. This means a zero of the system locates at about -3 in the complex plane; note that the choice of the zero at -3 is, in a sense, arbitrary. Then, the PD controller, $C_M(s)$, is expressed as below.

$$C_M(s) = -k_p \left(\frac{k_d}{k_p} s + 1 \right) = -k_p (0.3s + 1)$$

The proportional gain, k_p , is chosen as 0.3 by Root Locus with settling time of less than 1.5 sec. and less than 5% overshoot based on the operation angle 60 degree and the mass 1kg as shown in Figure 3.2; the operation angle and mass were chosen as the average values of the range of the link angle and the mass of the end-effector. The system has the settling time of less than 1.5 sec. when the poles (red *) of the closed loop system are placed in the left side of the blue dotted line.

However, the performance of the system such as overshoot and settling time changes depending on the angle and mass. Figure 3.3 shows the variation of poles of the closed loop system when the angle and mass are changed among their ranges, from 30 to 150 degrees, and from 0.35kg to 2kg; the blue * are poles when the angle and mass are 90 degrees and 0.35kg, and the red * are poles when the angle and mass are 30 degrees and 2kg. This indicates that the chosen controller does not make the system unstable, even though the overshoot and the settling time of the system increase depending on the mass and the angle.

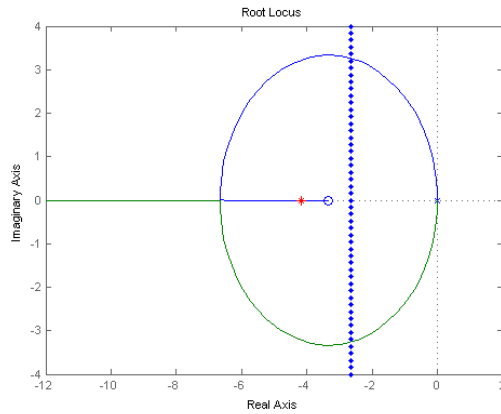


Figure 3-2: Root locus of $G(s)C_M(s)$; there are two poles of closed loop system, but in this figure, one of the poles is out of the range in left half plane of frequency domain

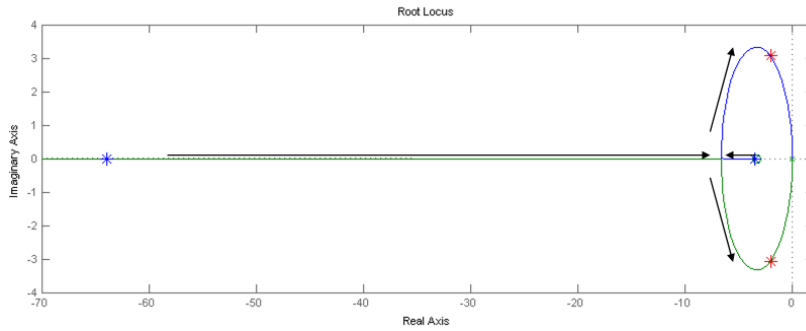


Figure 3-3: Variation of the closed loop system when mass and angle are changed between the boundary

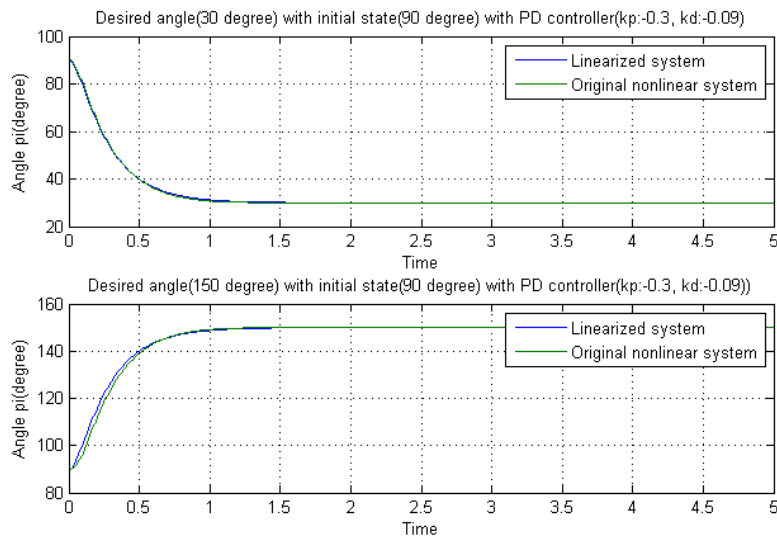


Figure 3-4: Compare of the linear model + PD controller and the nonlinear model + PD controller

Figure 3.4 shows the time responses of the linearized model and the nonlinear model with the chosen controller. The simulations are similar in the operational angle range when the system is in static balance. Thus, the linearized system can be used to design a controller.

The designed controller is simulated with the original nonlinear system as shown in Figure 3.5. When the link moves from 60 degree to 90 degree with mass variation from 0.35kg to 2kg at 5 sec., the macro actuator moves the lead nut of the system to static balance position following the mass variation, but the link has a steady state error due to the mass variation. The error can be removed by adding an integral controller. Assuming that the integral frequency is about 3 rad/sec to place the zero at same place of the previous PD controller and the damping ratio is 1 to suppress overshoot, the PID controller, $C_M(s)$, is expressed as below; in this case, mass of the lead nut is not considered for simple calculation.

$$C_M(s) = \frac{-K(s+3)^2}{s}$$

The gain, K , is designed as 0.2 by using the Root Locus Toolbox such that the settling time is 1.5 sec. and overshoot is less than 5%. As shown in Figure 3.6, the macro actuator can control the link without steady state error, and it converges to static balancing point. Thus, this closed loop system has adaptivity against mass variation, and the macro actuator can control the link as well. This means that the system with PID controller is asymptotically stable in the operational range. This can be confirmed by time responses of the system. It cannot be proven by stability analysis method such as Lyapunov direct method with sector nonlinearity and vanishing perturbation in Appendix A due to the existence of an affine model in the closed loop system.

The micro actuator is added to improve the performance of the macro actuating system. In this case, the control inputs are force, F , and torque, τ , which are applied to the two joints. Thus, the equation 3-1 are re-linearized with equilibrium point $(\infty, \frac{mgl}{kr})$, force of the macro actuator, and torque of the micro actuator as follows.

$$ml^2\ddot{\varphi} + kar \sin \varphi_e = \tau$$

$$(kr \sin \varphi_e)\varphi + ka = F$$

The transfer function $\frac{\varphi}{F}$ and $\frac{\varphi}{\tau}$ is expressed as follows.

$$\frac{\varphi(s)}{F(s)} = \frac{-r \sin \varphi_e}{ml^2s^2 - k(r \sin \varphi_e)^2} \quad \frac{\varphi(s)}{\tau(s)} = \frac{1}{ml^2s^2 - k(r \sin \varphi_e)^2}$$

Using these transfer functions, three control schemes are simulated and compared in next sections.

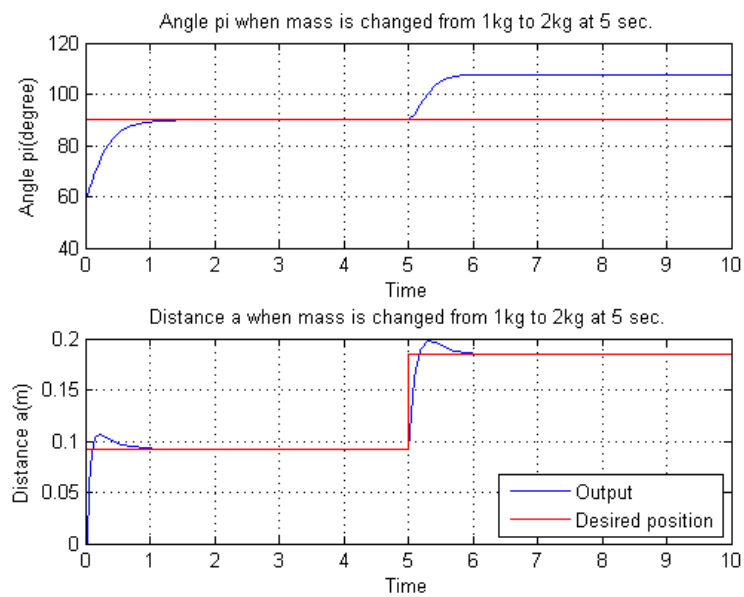


Figure 3-5: Responses of the closed loop system with PD controller when the mass changes from 1kg to 2kg at 5 sec.

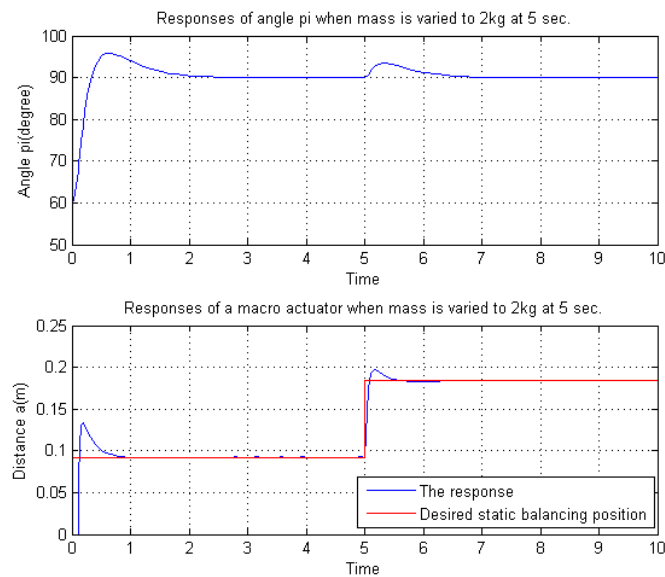


Figure 3-6: Responses of the closed loop system with PID controller when the mass changes from 1kg to 2kg at 5 sec.

3-3 Tracking/Compensating mode

The first control scheme is Tracking/Compensating mode shown in Figure 3.7. Macro-micro actuators control the angle of the link with a PID controller and a PD controller respectively. The PID controller of the macro actuator and the PD controller of the micro actuator are designed to have both 1.5 second settling time based on the operation angle 60 degree and the mass 1kg. Those controllers are designed through Root Locus Toolbox of Matlab with the previous two transfer functions; where $C_M(s)$ is the PID controller of $\frac{\varphi(s)}{F(s)}$, and $C_m(s)$ is the PD controller of $\frac{\varphi(s)}{\tau(s)}$

$$C_M(s) = -400 \frac{0.33^2 s^2 + 0.67s + 1}{s} \quad C_m(s) = 7(0.3s + 1)$$

These two controllers influence the other actuators due to coupling as shown in Figure 3.8. This figure is the step responses of three transfer functions with an unit step input: transfer function $\frac{\varphi(s)}{\tau(s)}$, $\frac{a(s)}{\tau(s)}$ and $\frac{\varphi(s)}{F(s)}$. $\frac{a(s)}{F(s)}$ is neglected since it is the open loop transfer function and the performance is determined by $\frac{\varphi(s)}{F(s)}$. The response of $\frac{a(s)}{\tau(s)}$ shows that the micro actuator influences to the leadscrew nut motion for a few seconds, but not a lot in full simulation time. The Macro actuator controls the angle and the micro actuator decreases the initial tracking error. This analysis of the linearized model can be confirmed with the original nonlinear model.

Figure 3.9 shows the responses of the nonlinear model with the first control scheme and the errors of the macro-micro actuated system comparing with the macro actuated system. The macro-micro actuated system estimates the mass variation. The macro actuator moves the link to the desired position with operating the leadscrew nut to the static balancing position. The micro actuator helps the macro actuator to diminish the tracking error. However, there are some influences in the performance of the system due to the coupling of the two actuators; the overshoot is smaller, but the settling time is larger than the performance of the macro actuated system.

This influence of the micro actuator can be explained clearly in the bode plot of Figure 3.10 and 3.11. When the PD controller of the micro actuator has relatively lower gains, the total system has low bandwidth and the system is governed by the macro actuator. On the other hands, when the gains of the PD controller are relatively higher, the total system has higher bandwidth, but the macro actuator has lower bandwidth. As a result, the micro actuator governs the system and increases the settling time of the system.

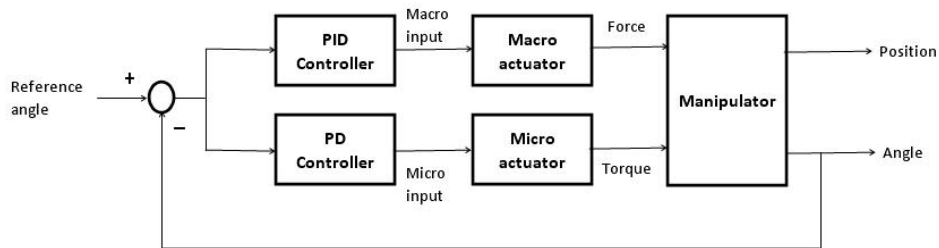


Figure 3-7: A block diagram of Tracking/Compensating mode

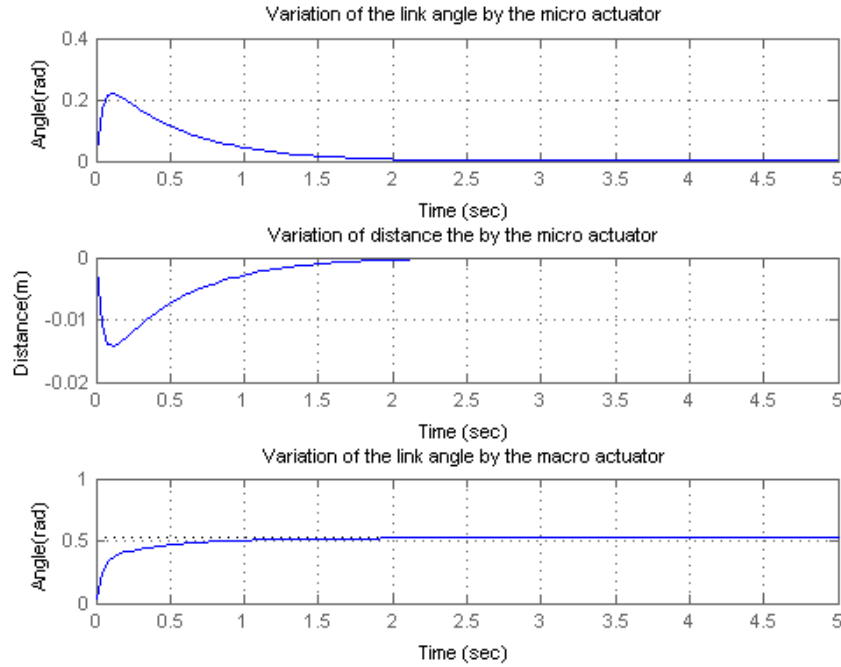


Figure 3-8: Time responses of multivariable system with Tracking/Compensating mode; the first view is response of $\frac{\varphi(s)}{\tau(s)}$, the second view is response of $\frac{a(s)}{\tau(s)}$, the third view is response of $\frac{\varphi(s)}{F(s)}$. The step input is $\frac{\pi}{6}$.

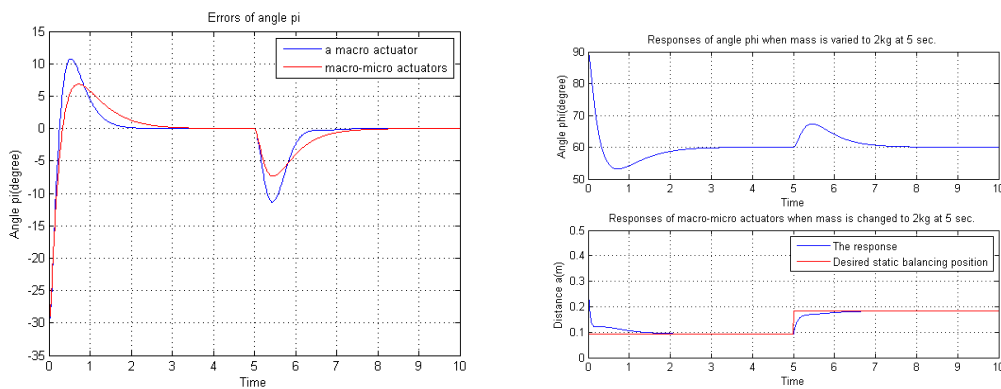


Figure 3-9: Comparison of errors and Response of macro-micro actuators when a mass is changed to 2kg at 5 sec.

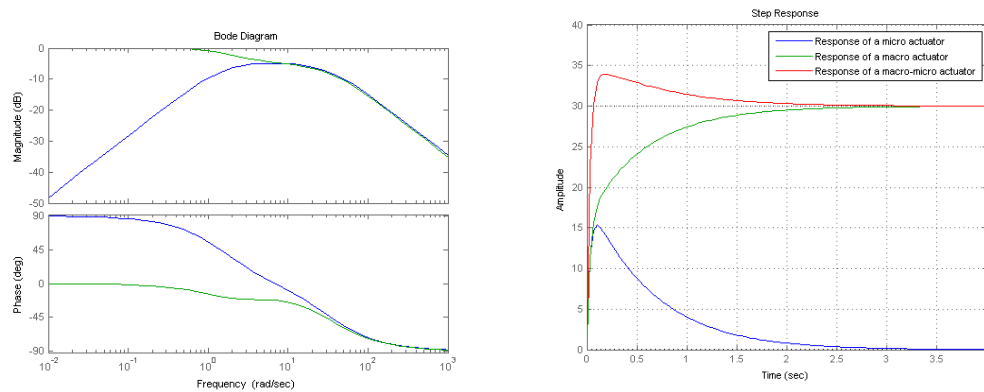


Figure 3-10: Bode plot and Step response of a closed loop system when $C_M(s) = -400 \frac{0.33^2 s^2 + 0.67s + 1}{s}$ and $C_m(s) = 7(0.3s + 1)$

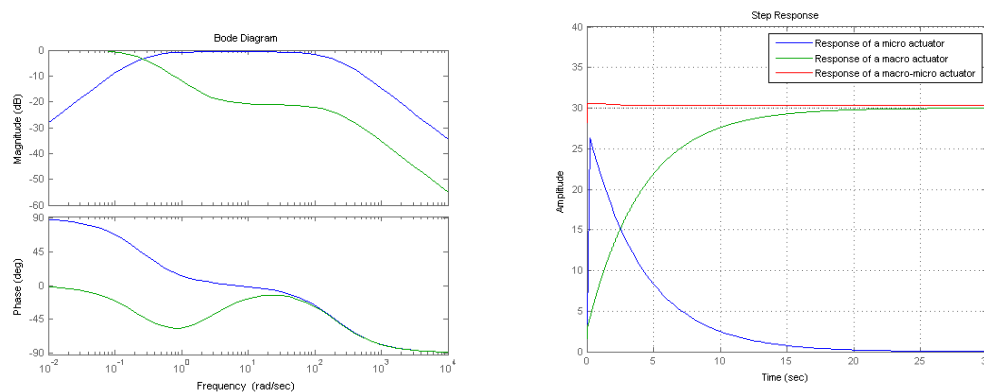


Figure 3-11: Bode plot and Step response of a closed loop system when $C_M(s) = -400 \frac{0.33^2 s^2 + 0.67s + 1}{s}$ and $C_m(s) = 70(0.3s + 1)$

However, the torque of the micro actuator increases and the static balance concept does not work for the total system since the settling time of the macro actuator decreases. Because of the interaction of two actuators, it is impossible to get both high bandwidth using this control scheme as shown in time responses of Figure 3.10 and 3.11. Moreover, if the actuator dynamics or the mass of the leadscrew nut in Figure 3.1 are added in motion equations, the system becomes a fourth order system and the PID controller of the macro actuator cannot control the link. These are proven in Appendix B. If the number of open loop poles exceeds the number of finite zeros by three or more, there is a value of the gain beyond which root loci enter the RHP; thus, the system can become unstable [6]. Thus, PID cascade controller has to be considered to control the fourth order system as shown in Appendix B.

3-4 Tracking/Tracking mode

The second control scheme is Tracking/Tracking mode, adding an integral controller to the PD controller of the micro actuator in the first control scheme as shown in Figure 3.12. The PID controller of the macro actuator and the PID controller of the micro actuator are designed to have both 1.5 second settling time based on the operation angle 60 degree and the mass 1kg using the Root Locus Toolbox of Matlab with the previous two transfer functions; where $C_M(s)$ is the PID controller of $\frac{\varphi(s)}{F(s)}$, and $C_m(s)$ is the PID controller of $\frac{\varphi(s)}{\tau(s)}$

$$C_M(s) = -400 \frac{0.33^2 s^2 + 0.67s + 1}{s} \quad C_m(s) = \frac{7(0.3s^2 + s + 1)}{s}$$

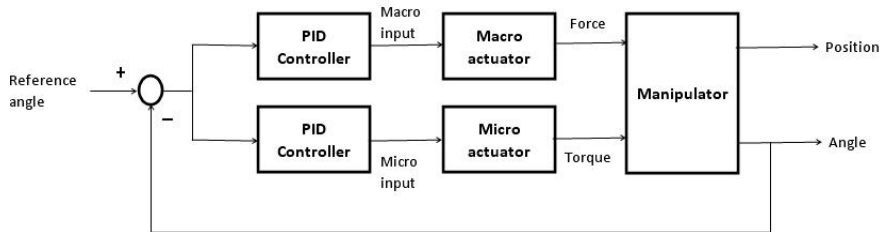


Figure 3-12: A block diagram of Tracking/Tracking mode

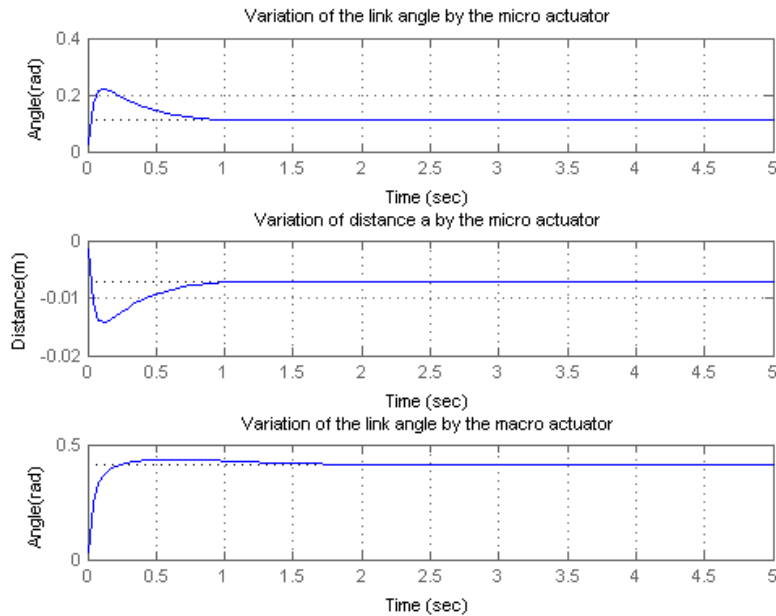


Figure 3-13: Time responses of the multivariable system with Tracking/Tracking mode; the first view is response of $\frac{\varphi(s)}{\tau(s)}$, the second view is response of $\frac{a(s)}{\tau(s)}$, the third view is response of $\frac{\varphi(s)}{F(s)}$. The step input is $\frac{\pi}{6}$.

These two controllers affect the motion of the macro-micro actuators as shown in Figure 3.13, but the interaction is not significant. This method shares the trajectory tracking of the link through the two PID controllers of the macro-micro actuators. The gains of the two controllers work as weighting values for the trajectory tracking as shown in the graphs of $\frac{\varphi(s)}{\tau(s)}$ and $\frac{\varphi(s)}{F(s)}$. For instance, when the gains of the micro actuator are larger, the micro actuator has more portion of trajectory tracking as shown in Figure 3.14. This is similar with Linear Quadratic Regulator (LQR) system. To have fast response of the system, the macro actuator has to have high bandwidth same as the previous control scheme. However, in practice, the macro actuator cannot have high bandwidth because of the given hardware condition such as the low pitch lead screw and voltage saturation, and the micro actuator has to consume its power always due to sharing the role of trajectory tracking.

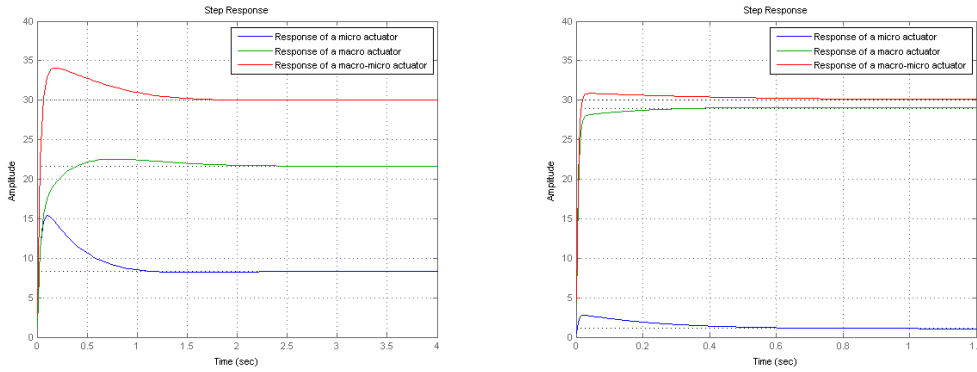


Figure 3-14: Step responses of a closed loop system when $C_M(s) = -400 \frac{0.33^2 s^s + 0.67s + 1}{s}$ and $C_m(s) = \frac{7(0.3s^2 + s + 1)}{s}$, and when $C_M(s) = -4000 \frac{0.33^2 s^s + 0.67s + 1}{s}$ and $C_m(s) = \frac{7(0.3s^2 + s + 1)}{s}$

3-5 Balancing/Tracking mode

Another method is to decide that the macro actuator should only control static balance. The macro actuator works only for static balance having a static balance point as an input and the micro actuator works for trajectory tracking as shown in Figure 3.15. The PID controller used for the macro actuator is same with the controller of the previous section, only changing the sign of the controller, since the feedback signal is different; the signs of $\frac{\varphi(s)}{F(s)}$ and $\frac{a(s)}{F(s)}$ are opposite. The PD controller of the micro actuator are designed to have both 1.5 second settling time based on the operation angle 60 degree and the mass 1kg through Root Locus Toolbox of Matlab and time responses of the multivariable system with the previous transfer functions; where $C_M(s)$ is the PID controller of $\frac{a(s)}{F(s)}$, and $C_m(s)$ is the PD controller of $\frac{\varphi(s)}{\tau(s)}$

$$C_M(s) = 400 \frac{0.33^2 s^s + 0.67s + 1}{s} \quad C_m(s) = 50(0.3s + 1)$$

An integral controller can be added to the PD controller of the micro actuator to compensate the steady state error by slow convergence of the macro actuator. This controller guarantees the stability of each plant with each input, but it does not show the stability of the multivariable system, in the view of the multivariable system. The stability of the multivariable system can be checked by the eigenvalues of the plant such as characteristic loci with Nyquist criterion theorem [7]. The characteristic loci of Figure 3.16 shows the system is stable with the above controllers, since one of eigenvalues is located in the right half plane (RHP) and the plot encircled (-1, 0) point one time in counter-clock-wise. This satisfies the Nyquist criterion theorem ($Z = N + P$); P is number of poles of loop gain in the RHP, Z is number of zeros of sensitivity function in the RHP, and N is number of (-1,0) clockwise encirclement. Figure 3.17 shows that the time responses of the stable multivariable system. There is some interaction between two actuators. The time responses of $\frac{a(s)}{\tau(s)}$ and $\frac{\varphi(s)}{F(s)}$ is caused by the interaction, but it can be removed by decoupling the system using a compensator [7].

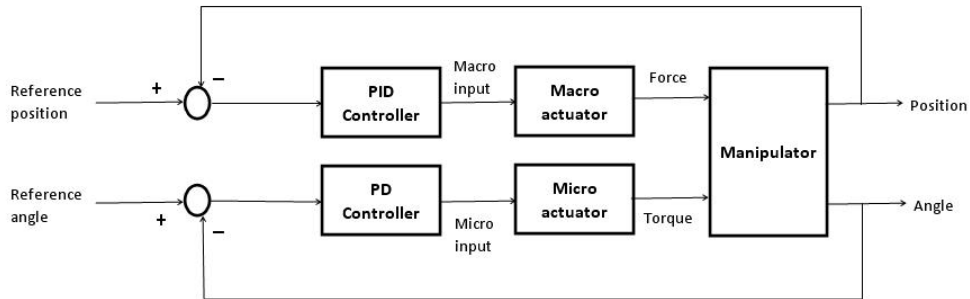


Figure 3-15: Block diagram of Balancing/Tracking mode

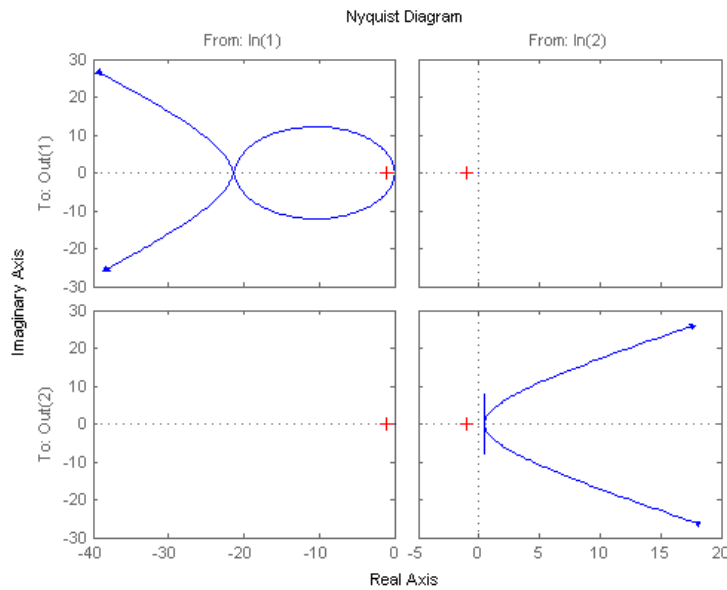


Figure 3-16: Characteristics loci

However, if the system has mass variation, the micro actuator needs lots of power to compensate error and the compensator decoupling the system does not work, since this mode cannot observe the mass variation as shown in Figure 3.18. Thus, an advanced algorithm has to be added to the control scheme. Also, the macro actuator has to have as high bandwidth as possible because the micro actuator has a load as much as the increased mass until the leadscrew nut converges to the static balancing point.

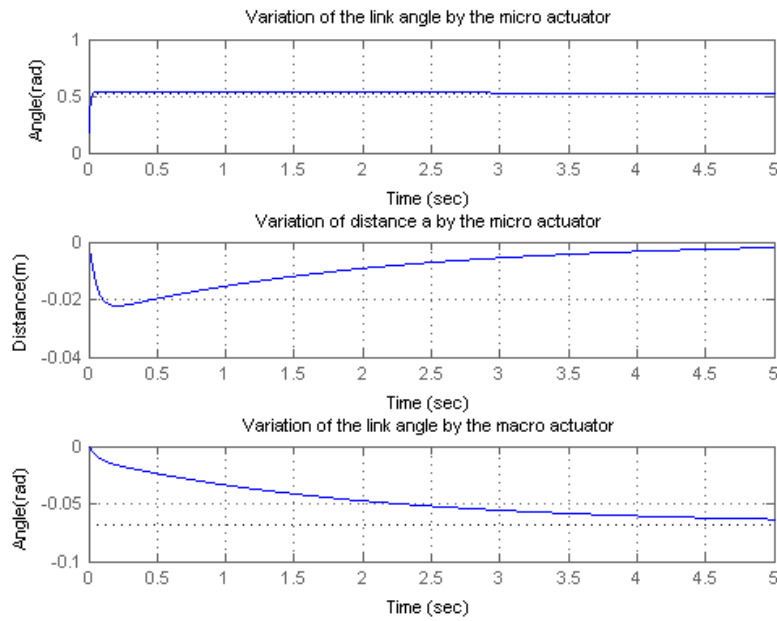


Figure 3-17: Time responses of the multivariable system with Balancing/Tracking mode; the first view is response of $\frac{\varphi(s)}{\tau(s)}$, the second view is response of $\frac{a(s)}{\tau(s)}$, the third view is response of $\frac{\varphi(s)}{F(s)}$. The step inputs are $\frac{\pi}{6}$ and static balancing point $(\frac{mgl}{kr})$ for the micro and macro actuators respectively.

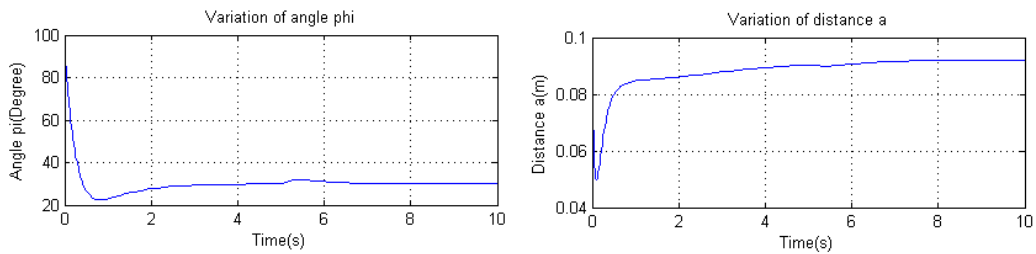


Figure 3-18: Time responses of macro-micro actuators when the mass is changed 1kg to 2kg at 5 sec. with $C_M(s) = 400 \frac{0.33^2 s^2 + 0.67s + 1}{s}$ and $C_m(s) = 50(0.2s^2 + s + 1)$

3-6 Comparison of three control schemes

In previous sections, the three control schemes were introduced and their characteristics were surveyed by time responses and frequency responses with PID controllers. The best scheme for the Delft robot arm is chosen by comparing the power of the micro actuator when the close loop system with the three control schemes has similar performance. As shown in Figure 3.19, the controllers of the three control schemes were designed as Table 3.3 to have similar performance with 1kg mass; the leadscrew nut is located at static balancing point for the mass. In that case, the micro actuator torque of Balancing/Tracking mode is the smallest except the initial surge torque. The initial surge torque can be removed by adding the trajectory planner such as cubic polynomial planner in Appendix C.

Schemes	The controller of the micro actuator	The controller of the macro actuator
Tracking/Compensating	$5(0.3s+1)$	$-400\frac{0.33^2s^2+0.67s+1}{s}$
Tracking/Tracking	$10\frac{0.3s+s+1}{s}$	$-400\frac{0.33^2s^2+0.67s+1}{s}$
Balancing/Tracking	$10\frac{0.2s+s+1}{s}$	$400\frac{0.33^2s^2+0.67s+1}{s}$

Table 3-3: Controllers of the three control schemes for step input

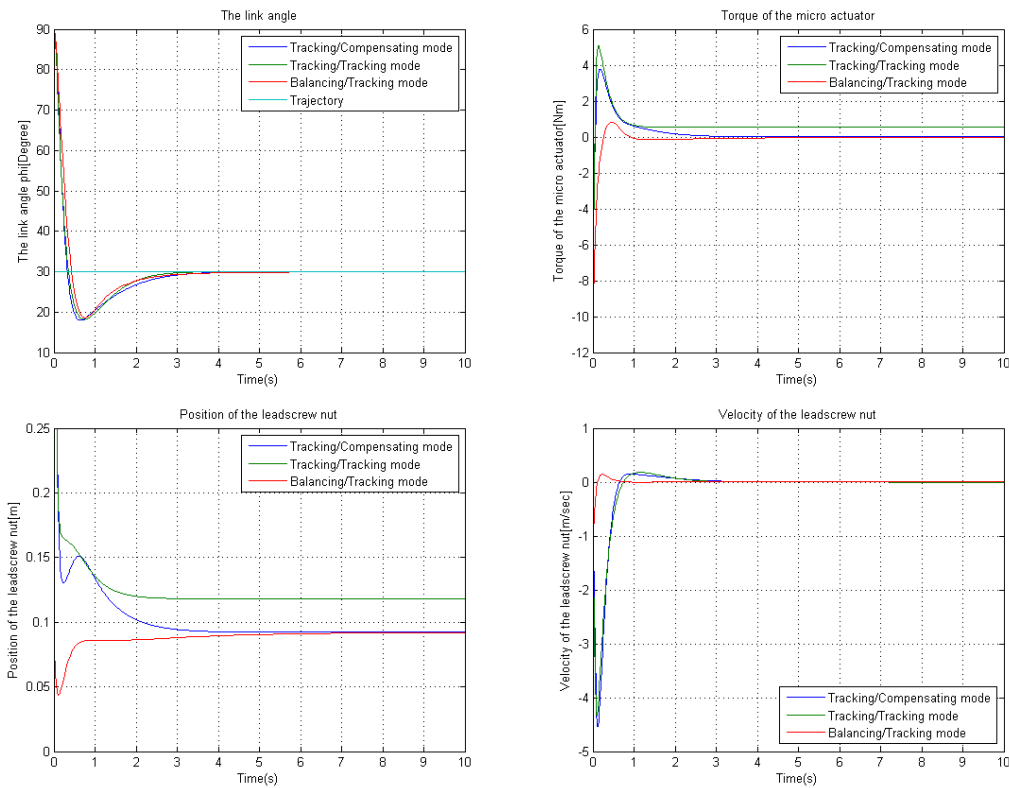


Figure 3-19: Step responses of macro-micro actuators

Figure 3.20 shows the time responses of the three control systems with the cubic polynomial trajectory. It is assumed that mass of the end-effector of the link is changed from 0.35kg to 2kg; the mass is observable, but the initial position of the leadscrew nut is a static balancing point for 0.35kg mass. The controllers of the three control schemes are same with the previous controllers of Table 3.3. As shown in Figure 3.20, the initial surge torques are removed by using the trajectory planner. The mode which has the smallest micro actuator torque is not Balancing/Tracking mode differently from the previous step responses. Moreover, it shows the worst trajectory tracking performance in the three control schemes. However, this simulation did not consider the maximum actuator velocity of the macro actuator with the leadscrew pitch, 0.00254m.

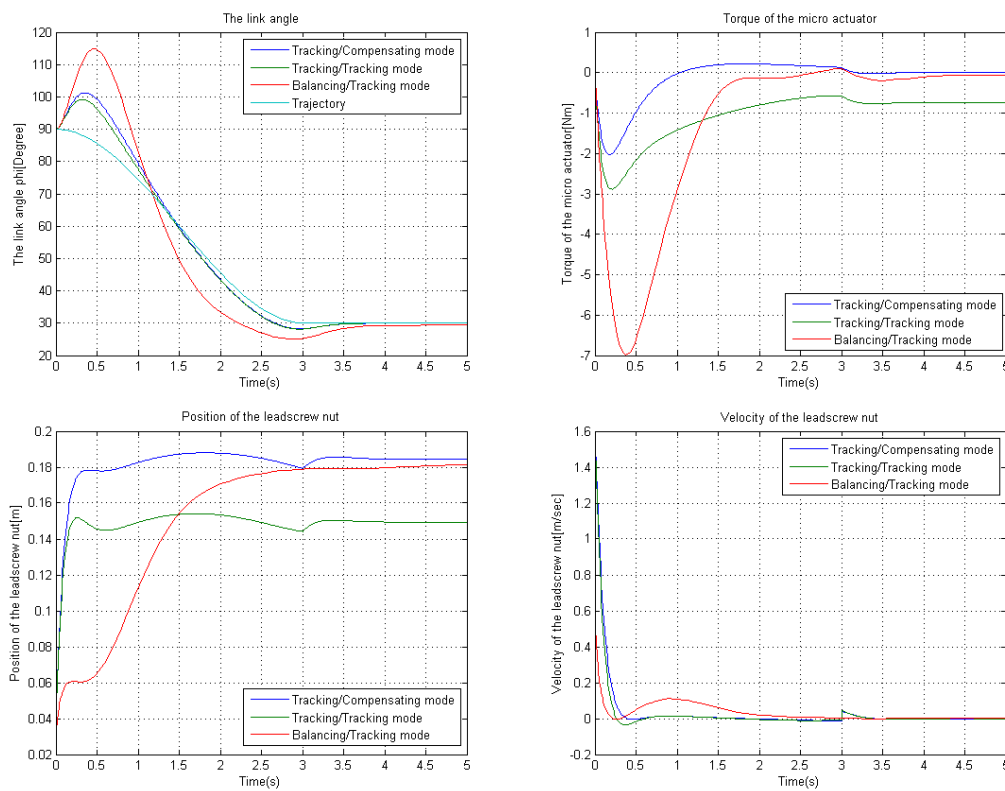


Figure 3-20: Time responses of macro-micro actuators

If the controller gains are tuned as Table 3.4 to make the three control schemes have same performance in boundary of the maximum velocity of the macro actuator, Balancing/Tracking mode shows the lowest torque of the micro actuator as shown in Figure 3.21 and Table 3.5. The leadscrew nut converges to the static balancing point, 0.184m. On the other hands, static balancing concept does not work in the other modes. The macro actuator performance and the micro actuator torque of Tracking/Compensating mode and Tracking/Tracking mode can be improved by decreasing the gains of the controller of the micro actuator. However, it results in worse performance of the link such as large tracking error. As a result, the best scheme for the purpose of the Delft robot arm is the Balancing/Tracking mode.

Schemes	The controller of the micro actuator	The controller of of the macro actuator
Tracking/Compensating	$120(0.3s+1)$	$-180 \frac{0.33^2 s^2 + 0.67s + 1}{s}$
Tracking/Tracking	$100 \frac{0.3s + s + 1}{s}$	$-130 \frac{0.33^2 s^2 + 0.67s + 1}{s}$
Balancing/Tracking	$100 \frac{0.2s + s + 1}{s}$	$350 \frac{0.33^2 s^2 + 0.67s + 1}{s}$

Table 3-4: Controllers of the three control schemes considering saturations for cubic polynomial trajectory

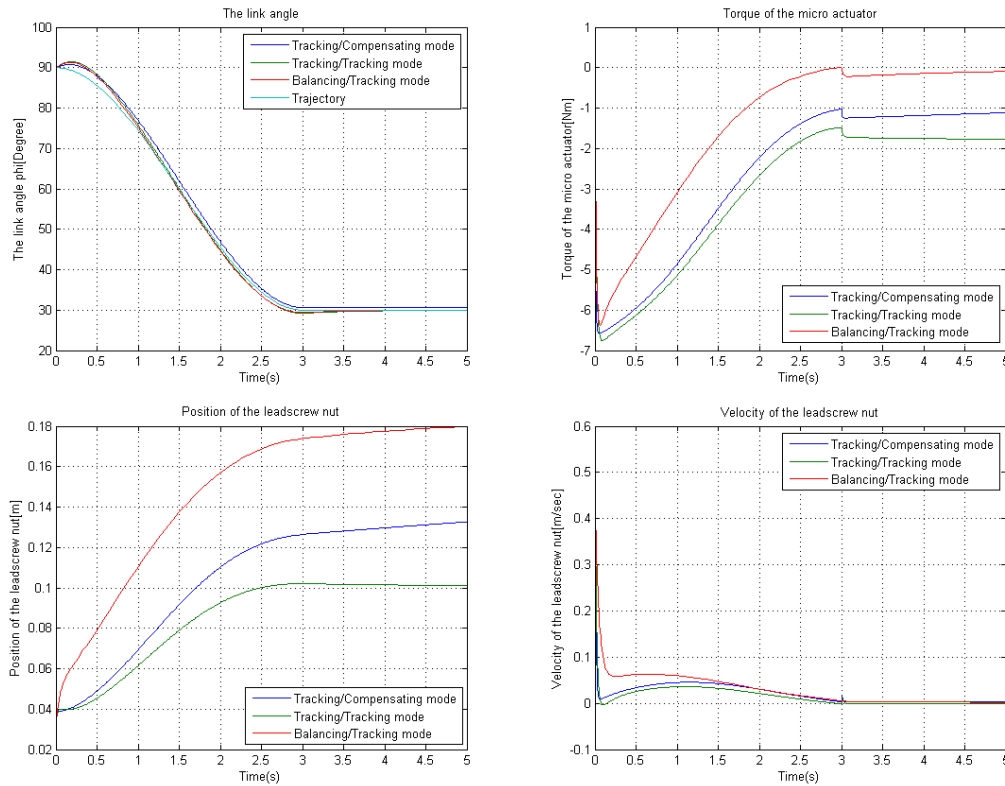


Figure 3-21: Time responses of macro-micro actuators

Schemes	The maximum torque of the micro actuator [Nm]	The final position of the leadscrew nut [m]	The maximum velocity of the macro actuator [m/sec]
Tracking /Compensating	6.60	0.13	0.47
Tracking /Tracking	6.73	0.10	0.45
Balancing /Tracking	6.35	0.18	0.45
Hardware saturations	-	-	0.50

Table 3-5: Comparison of the three control schemes

3-7 Conclusion

The three candidate control schemes for the single rotating link system were researched and compared through simulation. The first scheme, Tracking/Compensating mode, is good for simplicity of a control system, but this cannot achieve both high bandwidth of the macro actuator and the macro-micro actuated system. That is, there are trade-off between the two actuators depending on the gains of the controllers. Moreover, when the actuator dynamics or the mass of the lead screw nut are considered, a PID cascade controller has to be used. The PID cascade controller needs trial-and-error to tune the gains.

The second scheme uses both macro-micro actuators for trajectory tracking. Macro-micro actuators always work together for given task so that the performance follows the low bandwidth system between the macro actuator and the micro actuator. If the macro actuator has high bandwidth, then this can improve the performance sharing the trajectory tracking with the micro actuator. On the other hands, the macro actuator does not work for static balance since it shares the work compensating gravity with the micro actuator. The micro actuator always need torque to compensate a significant portion of gravity.

The third scheme makes the macro actuator work only for static balance. The micro actuator works only for trajectory tracking using distance a as the feedback signal of the macro actuator differently from the other schemes. This Balancing/Tracking mode with a linear controller showed better performance than the other modes, when hardware saturations are considered. However, the torque of the micro actuator depends on the speed of convergence of the macro actuator to the new static balancing point when the mass of the end-effector is changed. Moreover, it needs an advanced algorithm to estimate the mass variation of the end-effector in a non-autonomous system, while the other schemes do not need the advanced algorithm.

Chapter 4

Controller

The Balancing/Tracking mode with a linear controller showed better performance than the other modes in the previous chapter. However, in implementations of the linear controller, the linearization results in nonuniform damping throughout the workspace and other undesirable effects. When nonlinearities are not severe, local linearization can be used to derive linear models that are approximations of the nonlinear equations in the neighborhood of an operating point. Fortunately, the local linearization can work stable with the single rotating link system with the given conditions. However, its performance is changed depending on the mass and angle as shown in Figure 3.3 and Figure 4.1. To remove the performance variation, Feedback linearization is introduced. Feedback linearization method is to move the operating point with the manipulator as the manipulator moves, always linearizing about the desired position of the manipulator. The result of this moving linearization is a linear, but time-varying, system. It uses a nonlinear control term to cancel the nonlinearities in the controlled system so that the overall closed loop system is linear; this decouples the two actuators and gets rid of the nonlinearities of the system. However, an advanced algorithm such as adaptive or robust algorithms has to be implemented in the control scheme due to the decoupling and the properties of the Balancing/Tracking mode, which cannot estimate mass variation of the end-effector.

4-1 Feedback linearization control

This section shows the nonlinear control of the single rotating link system based on the third control scheme, which the macro actuator is for static balance and the micro actuator is for trajectory tracking. Motion equations of previous sections show that the system has nonlinearities with the coupling of the equations of the model. A nonlinear controller decouples and linearizes the dynamic model through a feedback linearization method. This method decouples the multivariable system even though the angle changes [8].

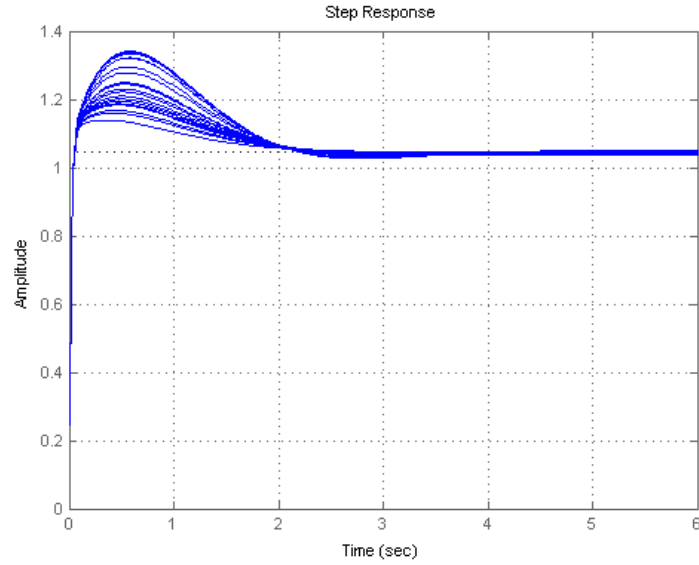


Figure 4-1: Step response depending on the variation of mass

Motion equations of the single rotating link system, equation 2-4, can be expressed as follows; M , C , and G are the mass inertia matrix, the vector of viscous damping and back EMF torques, and the vector of gravitational torques respectively.

$$M\ddot{q} + C\dot{q} + G = V \quad \text{where } q = [\beta \quad \theta]^T, \quad V = [V_m \quad V_M]^T \quad (4-1)$$

$$M = \begin{bmatrix} \frac{R_m}{k_i} (J_m + \frac{ml^2}{k_g^2}) & 0 \\ 0 & \frac{R_M J_M}{k_I} \end{bmatrix}$$

$$C = \begin{bmatrix} \frac{R_m B_m}{k_i} + k_b & 0 \\ 0 & \frac{R_M B_M}{k_I} + k_B \end{bmatrix}$$

$$G = \begin{bmatrix} \frac{R_m}{k_i k_g} (\frac{knr\theta}{k_G} - mgl) \sin \frac{\beta}{k_g} \\ \frac{R_M}{k_I k_G} (\frac{kn^2\theta}{k_G} - knr \cos \frac{\beta}{k_g}) \end{bmatrix}$$

As shown in the above matrix, two variables are coupled in the gravity part, G . The nonlinear matrix G is canceled by the feedback linearization method. Assuming that the angles and velocities of the single rotating link system are measurable and measurements are noiseless, the control law is defined as below. \hat{M} , \hat{C} , and \hat{G} are the estimates of M , C , and G respectively.

$$V = \hat{M}w(t) + \hat{C}\dot{q} + \hat{G} \quad (4-2)$$

Then, after substituting equation 4-1 into 4-2, deducing in the ideal case of a perfect modeling and in the absence of disturbances, the problem reduces to that of the linear control of two decoupled double-integrators:

$$\ddot{q} = w(t)$$

$w(t)$ is the new input control vector. Let $\ddot{q}_d(t)$, $\dot{q}_d(t)$, and $q_d(t)$ be the desired acceleration, velocity and position in the joint space. k_p and k_d are a proportional gain and a differential gain of a PD controller respectively. Both are (2×2) positive definite diagonal matrices. Defining $w(t)$ according to the following equation:

$$w(t) = \ddot{q}_d + k_d(\dot{q}_d - \dot{q}) + k_p(q_d - q)$$

Hence, referring to equation $\ddot{q} = w(t)$, the closed loop system response is determined by the following decoupled linear error equation:

$$\ddot{e} + k_d\dot{e} + k_p e = 0 \quad \text{where } e = q_d - q$$

Lyapunov candidate function is chosen as

$$E = \frac{1}{2}\dot{e}^T\dot{e} + \frac{1}{2}e^T k_p e$$

Using Lyapunov direct method,

$$E(e, \dot{e}) = E(0, 0) = 0$$

$$E(e, \dot{e}) > 0$$

$$\dot{E} = \dot{e}\dot{e} + \dot{e}k_p e$$

$$= (-k_p e^T - k_d \dot{e}^T)\dot{e} + \dot{e}^T k_p e$$

$$= -\dot{e}^T k_d \dot{e} < 0$$

$$E(\infty, \infty) > 0$$

Hence, the solution $e(t)$ of the error equation is globally stable. It implies that a closed loop system is globally asymptotically stable.

The block diagram of this control method is presented in Figure 4.2. The control inputs for the actuators include three components: the first compensates for viscous damping and gravity effects: the second is a proportional and derivative control with variable gains $\hat{M}k_p$ and $\hat{M}k_d$ respectively; and the third provides the predictive action of the desired acceleration torques $\hat{M}\ddot{q}_d$. Inputs of the micro actuator are a desired trajectory of the link with a velocity and an acceleration through trajectory planner, and the input of the macro actuator is a value, $\frac{mgl}{kr}$, which makes the link marginally stable at every angle. The controller governs the whole system as expressed in the above closed loop equation, and the gains of the controller are chosen to have no overshoot, given damping ratio 1.

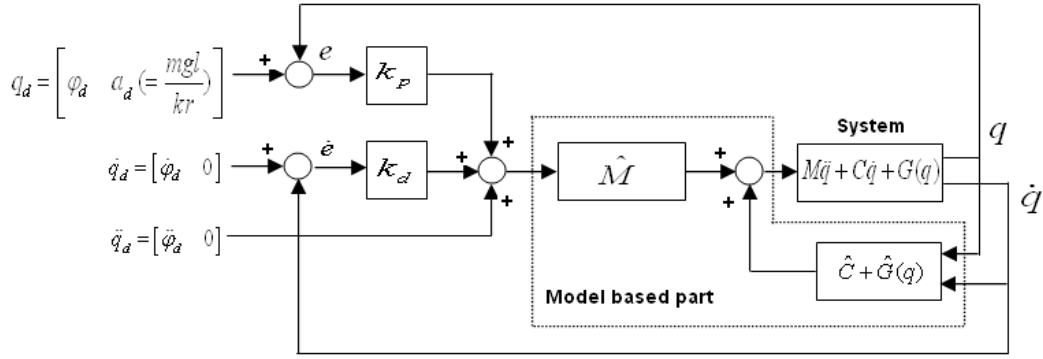


Figure 4-2: A block diagram of the feedback linearization control

The responses of the single rotating link system are shown in Figure 4.3. It shows that a higher gain controller with $k_p=10000$ and $k_d=200$ for the micro actuator, has a smaller tracking error than the lower gain controller with $k_p=100$ and $k_d=20$ for the micro actuator with the low torque of the micro actuator; controller gains of the macro actuator are $k_p=100$ and $k_d=20$ in this section. In the presence of modeling errors due to the payload, the closed loop equation is obtained by combining equations 4-1 and 4-2:

$$\begin{aligned} \hat{M}(\ddot{q}_d + k_d\dot{e} + k_p e) + \hat{C}\dot{q} + \hat{G} &= M\ddot{q} + C\dot{q} + G \\ \Rightarrow \ddot{e} + k_d\dot{e} + k_p e &= \hat{M}^{-1} \left[(M - \hat{M})\ddot{q} + (C - \hat{C})\dot{q} + (G - \hat{G}) \right] \end{aligned}$$

If the mass of the model of the single rotating link system is not accurate, the above equation will be expressed as the follows.

$$\ddot{e} + k_d\dot{e} + k_p e = \hat{M}^{-1}\tilde{M}\ddot{q} + \hat{M}^{-1}\tilde{G} \quad \text{where } \tilde{M} = M - \hat{M} \quad \text{and} \quad \tilde{G} = G - \hat{G} \quad (4-3)$$

In this equation, the modeling errors constitute an excitation for the error equation. To check the stability of the above closed loop system, Lyapunov candidate function is chosen as

$$E = \frac{1}{2}e^T\dot{e} + \frac{1}{2}e^T k_p e$$

Using Lyapunov direct method,

$$E(e, \dot{e}) = E(0, 0) = 0$$

$$E(e, \dot{e}) > 0$$

$$\dot{E} = \dot{e}\dot{e} + \dot{e}k_p e$$

$$= (-k_p e^T - k_d \dot{e}^T + \hat{M}^{-1}\tilde{M}\ddot{q})\dot{e} + \dot{e}^T k_p e$$

$$= (\hat{M}^{-1}\tilde{M}\ddot{q})\dot{e} - \dot{e}^T k_d \dot{e} < 0$$

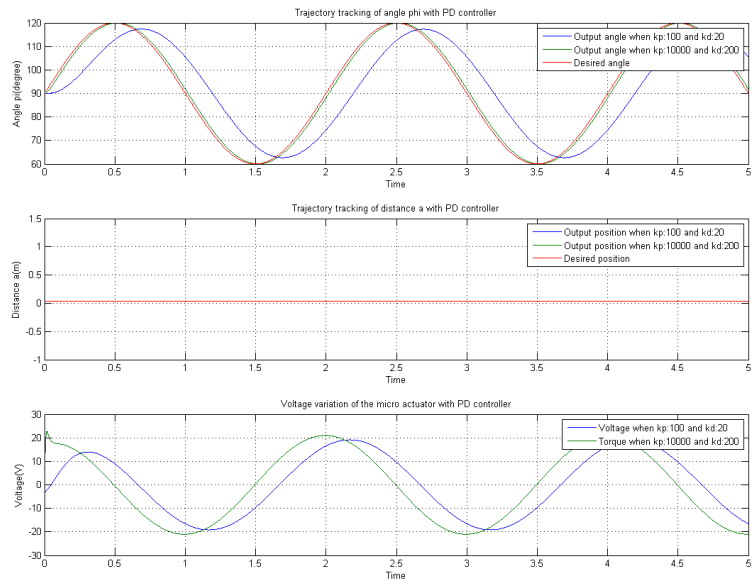


Figure 4-3: Responses with no modeling error

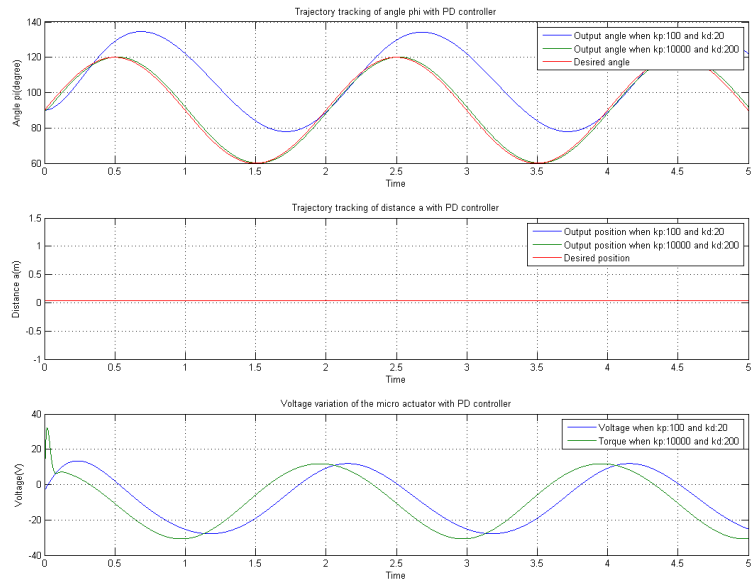


Figure 4-4: Responses with the modeling error(1kg)

The single rotating link system does not warrant that a tracking error becomes zero if there are modeling errors or the system is a non-autonomous system since \dot{E} is not always smaller than zero. If the modeling errors are large, it is necessary to increase the proportional and derivative gains as shown in Figure 4.4. Then, the system becomes robust against the modeling errors or the disturbance. However, there is a limitation in the high gain controller since the system cannot have voltage, current, and motor speed over the hardware saturations. Furthermore, the high gains amplifies a measurement noise, and the micro actuator spends its energy to compensate the increased mass, since the macro actuator does not work for static balance against the increased mass. For those reasons, an advanced algorithm, which makes the macro actuator move its position to balance the system against the mass variation of the payload, has to be added in the controller.

4-2 Sliding mode control

One of the most important approaches to dealing with model uncertainty is a sliding mode control [9, 10]. As shown in Figure 4.5, sliding mode approach is to drive the nonlinear plant's state trajectory onto a pre-specified surface in the state space and to maintain the plant's state trajectory on this surface for a subsequent time by the switching control law, which is derived by switching surface and Lyapunov function. The typical structure of this controller is composed of a nominal part, same as the feedback control law, and an additional term aimed at dealing with a model uncertainty. A sliding mode algorithm, which uses a sliding variable, is implemented for robustness of the single rotating link system.

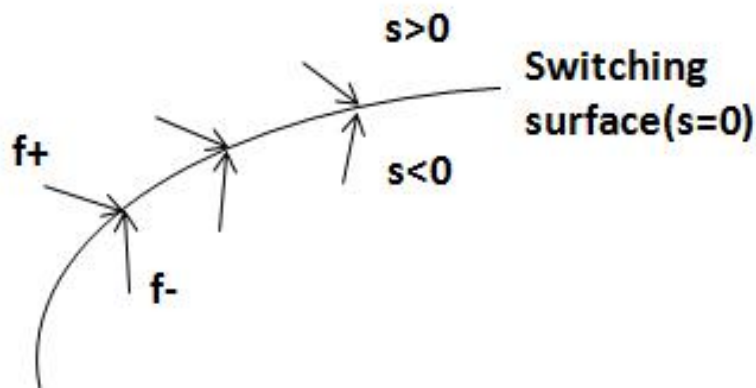


Figure 4-5: Concept of sliding mode control; f is a closed loop function

The principle of the sliding mode control scheme in Figure 4.6 is explained in short as follows. The micro actuator realizes the mass variation as a disturbance of a system so that the control input is increased to reject the disturbance. During the term of estimation, the macro actuator diminishes the mass error by switching feedback gains depending on the variation of sliding variables and moves to the distance, which makes the link in static balance. Finally, the motion of the macro actuator decreases the load of the micro actuator so that the torque of the micro actuator to compensates gravity and a trajectory error becomes approximately zero.

The sliding mode algorithm of the single rotating link system is derived as follows. As shown in equation 4-1, M and G matrices are affected by mass variation. Assuming that the angles and velocities of the single rotating link system are measurable and measurements are noiseless, the control law is defined as below. \hat{M} , \hat{C} , and \hat{G} are the estimates of M , C , and G respectively.

$$V = \hat{M}w(t) + \hat{C}\dot{q} + \hat{G} \tag{4-4}$$

Then, after substituting equation 4-1 into 4-4, deducing in the absence of disturbances, the closed loop equation with modeling errors is expressed as below.

$$M\ddot{q} + C\dot{q} + G = \hat{M}w(t) + \hat{C}\dot{q} + \hat{G} \tag{4-5}$$

where $w(t)$ is the new input control vector.

Let $\ddot{q}_d(t)$, $\dot{q}_d(t)$, and $q_d(t)$ be the desired acceleration, velocity and position in the joint space, and let s be a sliding variable, which replaces a n^{th} order tracking problem in q with a 1st order stabilization problem in s . Defining $w(t)$ according to the following equation with a strict positive constant λ : where $s = \dot{e} + \lambda e = \dot{q} - \dot{q}_d + \lambda e = \dot{q} - \dot{q}_r$ and $\dot{q}_r = \dot{q}_d - \lambda e$

$$w(t) = \ddot{q}_r - k_d s - k_p e$$

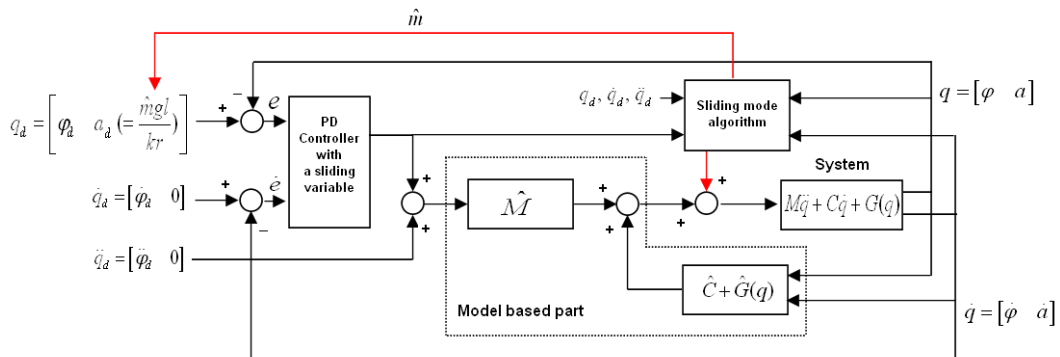


Figure 4-6: Control structure of the robust feedback linearization control

Equation 4-5 is re-written as follows.

$$\begin{aligned}
M\ddot{q} + C\dot{q} + G &= \hat{M}(\ddot{q}_r - k_d s - k_p e) + \hat{C}\dot{q} + \hat{G} \\
\Rightarrow M\ddot{q} + C\dot{q} + G - M\ddot{q}_r &= \hat{M}(\ddot{q}_r - k_d s - k_p e) + \hat{C}\dot{q} + \hat{G} - M\ddot{q}_r \\
\Rightarrow M\dot{s} + \hat{M}k_d s + \hat{M}k_p e &= \tilde{M}\ddot{q}_r + \tilde{G}
\end{aligned}$$

To check the stability of a closed loop system, Lyapunov candidate function is chosen as

$$E = \frac{1}{2}s^T M s + \frac{1}{2}e^T \hat{M}k_p e$$

Using Lyapunov direct method,

$$E(s, e) = E(0, 0) = 0$$

$$E(s, e) > 0$$

$$\begin{aligned}
\dot{E} &= \dot{s}M s + \dot{e}\hat{M}k_p e \\
&= (-\hat{M}k_d s - \hat{M}k_p e + \tilde{M}\ddot{q}_r + \tilde{G})s + \dot{e}^T \hat{M}k_p e \\
&= -s^T \hat{M}k_d s - s^T \hat{M}k_p e + (\tilde{M}\ddot{q}_r + \tilde{G})s + \dot{e}^T \hat{M}k_p e \\
&= -s^T \hat{M}k_d s - (\dot{e} + \lambda e)^T \hat{M}k_p e + (\tilde{M}\ddot{q}_r + \tilde{G})s + \dot{e}^T \hat{M}k_p e \\
&= -s^T \hat{M}k_d s - e^T \lambda \hat{M}k_p e + (\tilde{M}\ddot{q}_r + \tilde{G})s
\end{aligned}$$

To make the closed loop system stable, $-s^T \hat{M}k_d s - e^T \lambda \hat{M}k_p e + (\tilde{M}\ddot{q}_r + \tilde{G})s$ has to be smaller than zero. The first and second factors are always smaller than zero when k_p and k_d are positive. However, the third factor does not warrant a negative value because parameter values can be changed. Thus, for the stability of the system, \tilde{M} and \tilde{G} have to follow the below conditions to make the system stable.

$$\left(\begin{array}{l} \text{if } s\ddot{q}_r > 0, \tilde{M} = -|\rho_1| \\ \text{if } s > 0, \tilde{G} = -|\rho_2| \end{array} \right)$$

$$\left(\begin{array}{l} \text{if } s\ddot{q}_r < 0, \tilde{M} = |\rho_1| \\ \text{if } s < 0, \tilde{G} = |\rho_2| \end{array} \right)$$

$$\text{where } \tilde{M} = \begin{bmatrix} \rho_1 \\ 0 \end{bmatrix} = \begin{bmatrix} \frac{R_m}{k_i}(\hat{m} - m)l^2 & 0 \\ 0 & 0 \end{bmatrix}, \quad \tilde{G} = \begin{bmatrix} \rho_2 \\ 0 \end{bmatrix} = \begin{bmatrix} -\frac{R_m}{k_i k_g}(\hat{m} - m)gl \sin \varphi \\ 0 \end{bmatrix}$$

Assuming the end-effector of the link can be changed from 0.35kg to 2 kg, the present study adds control inputs to compensate the tracking error resulted from the mass variation as below.

$$\begin{cases} \text{if } s\ddot{q}_r > 0, \tilde{M} = \begin{bmatrix} \frac{R_m - 1.65l^2}{k_i k_g^2} & 0 \\ 0 & 0 \end{bmatrix} \\ \text{if } s < 0, \tilde{G} = \begin{bmatrix} \frac{R_m}{k_i k_g} (-1.65gl \sin \frac{\beta}{k_g}) \\ 0 \end{bmatrix} \end{cases}$$

$$\begin{cases} \text{if } s\ddot{q}_r < 0, \tilde{M} = \begin{bmatrix} \frac{R_m}{k_i k_g^2} & 0 \\ 0 & 0 \end{bmatrix} \\ \text{if } s > 0, \tilde{G} = \begin{bmatrix} \frac{R_m}{k_i k_g} (1.65gl \sin \frac{\beta}{k_g}) \\ 0 \end{bmatrix} \end{cases}$$

The above rules are implemented in the sliding mode algorithm block of Figure 4.6 with the following controller gains and sliding constant.

$$K_p = \begin{bmatrix} 900 & 0 \\ 0 & 16 \end{bmatrix}, \quad K_d = \begin{bmatrix} 60 & 0 \\ 0 & 8 \end{bmatrix}, \quad \lambda = \begin{bmatrix} 10 \\ 0.1 \end{bmatrix}$$

However, as shown in the above sliding mode algorithm, the micro actuator only realizes the mass variation and has additional control inputs, but the input of the macro actuator can not estimate the mass variation since there is no feedback of mass variation for the input. Therefore, the static balancing concept does not work as shown in Figure 4.7 because the macro actuator does not have motion for the increased mass. The voltage of the micro actuator is not decreased also because the micro actuator has to compensate an error caused by the mass variation. Thus, some factor has to be added to realize the mass variation for a macro actuator. The additional algorithm is derived from the variation of the gravity torque.

$$\begin{cases} \text{if } \begin{bmatrix} \frac{R_m}{k_i k_g} (\frac{knr\theta}{k_G} - mgl) \sin \frac{\beta}{k_g} \\ 0 \end{bmatrix} + \tilde{G} > 0, \hat{m} = -2 \\ \text{if } \begin{bmatrix} \frac{R_m}{k_i k_g} (\frac{knr\theta}{k_G} - mgl) \sin \frac{\beta}{k_g} \\ 0 \end{bmatrix} + \tilde{G} < 0, \hat{m} = 2 \end{cases}$$

The above rule is implemented in the sliding mode algorithm block with the previous rules. Then, the macro actuator estimates the mass and updates the input of the macro actuator and the model based part of the controller. However, the voltage of the micro actuator still has chattering phenomena because of the switching of the above rules, as shown in Figure 4.8. To decrease the high frequency chattering, a low pass filter, $\frac{10}{s+10}$, is implemented in the sliding mode algorithm. As a result, the macro actuator realizes the mass variation and moves its distance for static balancing as shown in Figure 4.9. The voltage of the micro actuator is also decreased due to the recognition of the mass variation of the macro actuator.

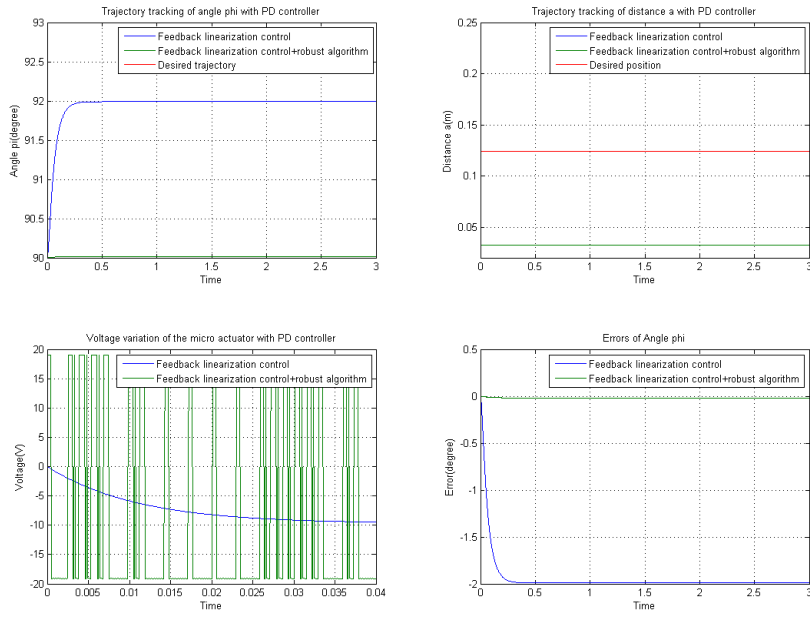


Figure 4-7: Responses of the feedback linearization control and the robust feedback linearization control with a modeling error (1kg) to keep the initial angle (90 degree)

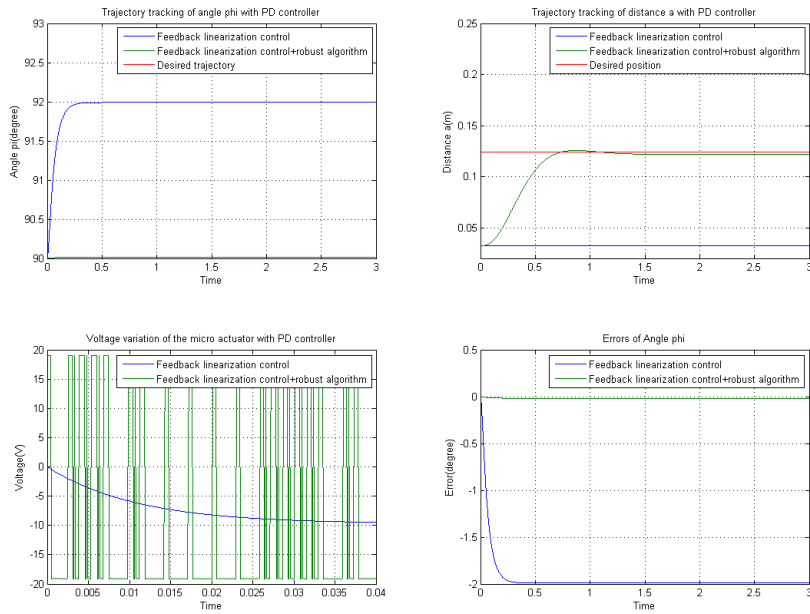


Figure 4-8: Responses of the feedback linearization control and the robust feedback linearization control with a modeling error (1kg) to keep the initial angle (90 degree)

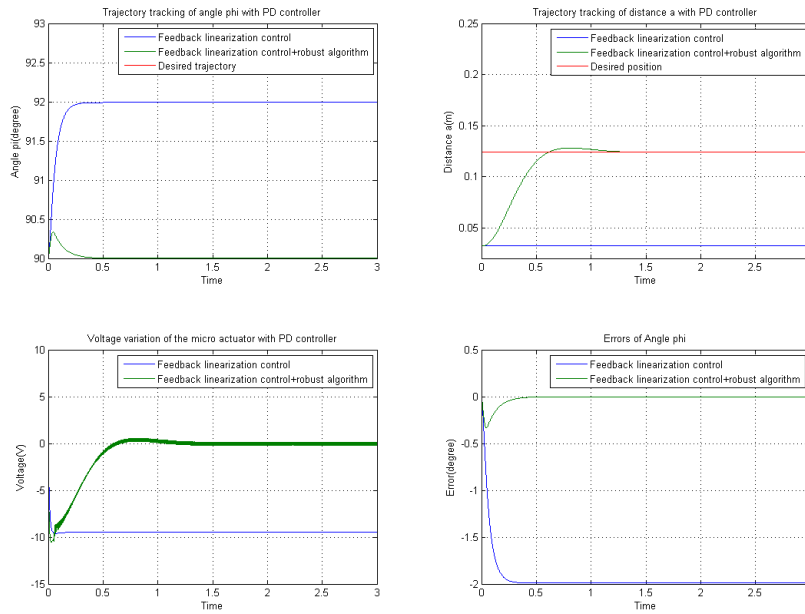


Figure 4-9: Responses of the feedback linearization control and the robust feedback linearization control with a modeling error (1kg) to keep the initial angle (90 degree)

4-3 Indirect adaptive control

An indirect adaptive algorithm, which uses a prediction error and the least squares method, is implemented to estimate the mass variation of the payload of the single rotating link system [9, 10]. Figure 4.10 shows the indirect adaptive control scheme, and its principle is explained in short as follows. The micro actuator estimates the mass variation as a disturbance of the system so that the input of the micro actuator is increased to reject the disturbance. The macro-micro actuators estimate the mass variation from the prediction error and the least squares method, and the macro actuator moves the leadscrew nut to the static balance position. This prediction error concept is explained as below with considering the input of the single rotating link system, which is defined in equation 4-1.

$$V = M\ddot{q} + C\dot{q} + G(q) \quad (4-6)$$

Given some estimate \hat{V} of the parameters, a prediction \hat{V} of V is

$$\hat{V} = \hat{M}\ddot{q} + \hat{C}\dot{q} + \hat{G}$$

Then, the prediction error ϵ of the input is given by

$$\begin{aligned} \epsilon &= V - \hat{V} \\ &= V - [\hat{M}\ddot{q} + \hat{C}\dot{q} + \hat{G}(q)] \end{aligned}$$

Unfortunately, the generation of ϵ requires the measurement of \ddot{q} . However, the acceleration signal is eliminated by filtering both \hat{V} and V as shown in Figure 4.11. Providing that ϵ is filtered by a stable and proper low pass filter with the transfer function of the system, $H(s)$ is

$$H(s) = \frac{\omega}{s + \omega} \quad \text{where } \omega > 0$$

The filter output is

$$\epsilon_f(s) = H(s)\epsilon(s)$$

Then, a filtered prediction error is

$$\begin{aligned} \epsilon_f(s) &= H(s)\epsilon(s) = H(s)V(s) - H(s)(\hat{M}(s)s^2q(s) + \hat{C}(s)sq(s) + \hat{G}(s)) \\ &= V_f(s) - (H(s)s\hat{M}(s)sq(s) + H(s)\hat{C}(s)sq(s) + H(s)\hat{G}(s)) \end{aligned}$$

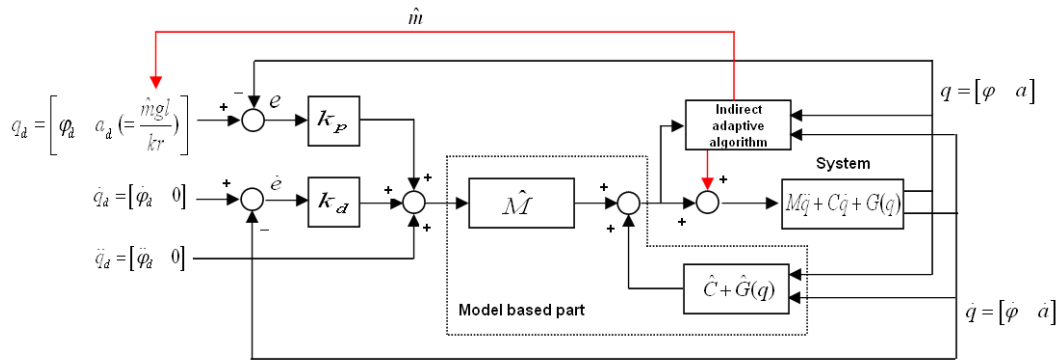


Figure 4-10: Control structure of the indirect adaptive feedback linearization control

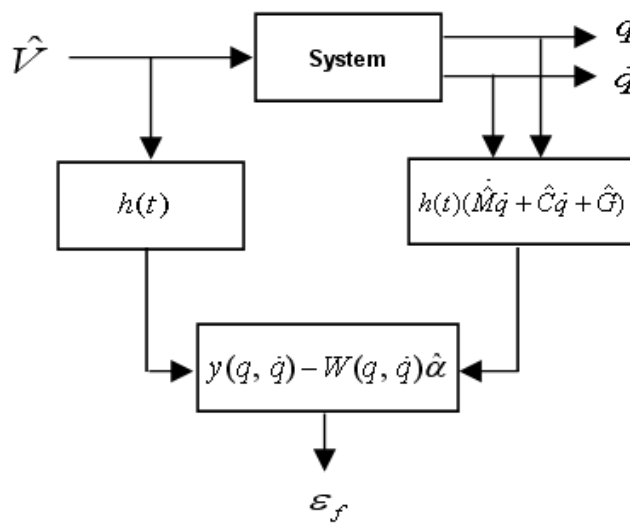


Figure 4-11: Generation of the filtered prediction error on the control torque

Obtaining the inverse Laplace transform,

$$\epsilon_f(q, \dot{q}) = V_f(q, \dot{q}) - (h(t)\dot{M}\dot{q} + h(t)\hat{C}\dot{q} + h(t)\hat{G}(q)) = y(q, \dot{q}) - W(q, \dot{q})\hat{m} \quad (4-7)$$

where $y(q, \dot{q}) = \hat{V}_f(q, \dot{q})$ and $W(q, \dot{q})\hat{m} = h(t)\dot{M}\dot{q} + h(t)\hat{C}\dot{q} + h(t)\hat{G}(q)$

$W(q, \dot{q})$ is a filtered regressor matrix, and \hat{m} is the estimate of mass of the end-effector. In the standard least-squares method, the estimate of the parameter is generated by minimizing the total prediction error with respect to $\hat{m}(t)$.

$$J = \int_0^t \|y(r) - W(r)\hat{m}(r)\|^2 dr$$

Since this implies the fitting of all the past data, this estimate potentially has the advantage of averaging out the effects of measurement noise. The equation, $\|y(r) - W(r)\hat{m}(r)\|^2$, has to be minimized to have low cost function, J . The cost function of J can be written as

$$\begin{aligned} \epsilon_f \epsilon_f &= (y - W\hat{m})(y - W\hat{m}) \\ &= y^T y - y^T W\hat{m} - \hat{m}^T W^T y + \hat{m}^T W^T W\hat{m} \\ &= y^T y - y^T W\hat{m} - \hat{m}^T W^T y + \hat{m}^T W^T W\hat{m} + y^T W(W^T W)^{-1} W^T y - y^T W(W^T W)^{-1} W^T y \\ &= y^T (I - W(W^T W)^{-1} W^T) y + (\hat{m} - (W^T W)^{-1} W^T y)^T W^T W (\hat{m} - (W^T W)^{-1} W^T y) \end{aligned}$$

The first term on the right hand side is independent of \hat{m} . The second term is always positive. The minimum is obtained for

$$\hat{m} = (W^T W)^{-1} W^T y$$

Then, the above normal equation can be written as

$$\hat{m}(t) = [\int_0^t W^T W dr]^{-1} \int_0^t W^T y dr \quad (4-8)$$

The derivative of equation 4-8 with respect to time is expressed as

$$\begin{aligned} \frac{d}{dt}[P^{-1}(t)]\hat{m} + P^{-1}\dot{\hat{m}} &= W y \\ P^{-1}\dot{\hat{m}} &= W y - W^T W\hat{m} = W(y - W^T \hat{m}) = -W^T \epsilon_f \\ \text{where } P(t) &= [\int_0^t W^T(r)W(r)dr]^{-1} \end{aligned}$$

Then, the parameter update satisfies

$$\dot{\hat{m}} = -P(t)W^T \epsilon_f \quad (4-9)$$

with $P(t)$ being called the estimator gain matrix. In the implementation of the estimator, it is desirable to update the gain P directly. By using the identity

$$\frac{d}{dt}[PP^{-1}] = \dot{P}P^{-1} + P\frac{d}{dt}[P^{-1}] \Rightarrow \dot{P} = -PW^T WP \quad (4-10)$$

The above algorithms, 4-7, 4-9 and 4-10, are implemented in the indirect adaptive algorithm block in Figure 4.10 with the following controller gains.

$$K_p = \begin{bmatrix} 900 & 0 \\ 0 & 16 \end{bmatrix}, \quad K_d = \begin{bmatrix} 60 & 0 \\ 0 & 8 \end{bmatrix}$$

The macro actuator estimates the mass variation and moves its distance for static balancing as shown in Figure 4.12. The voltage of the micro actuator is also decreased due to the estimation of the mass variation of the macro actuator.

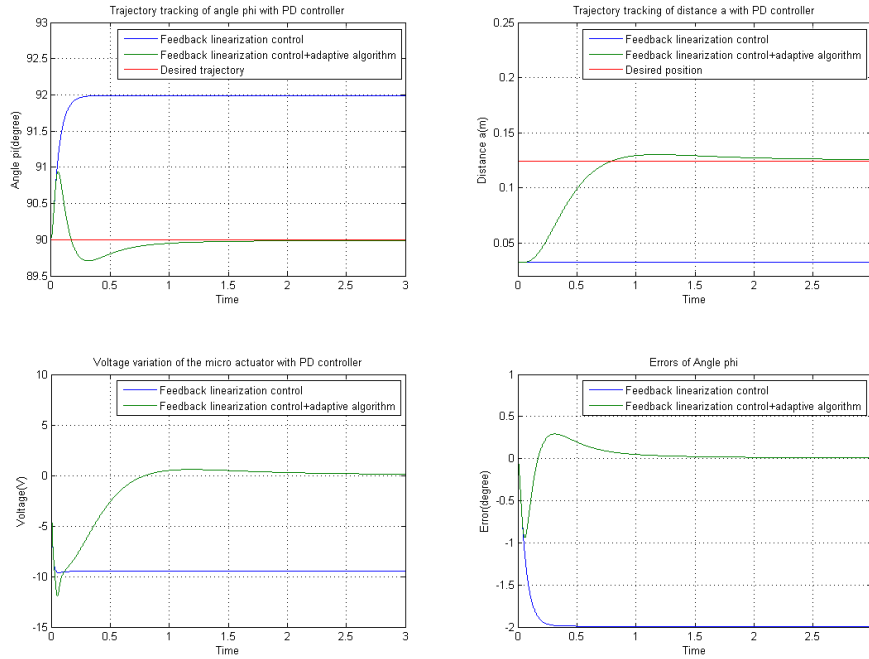


Figure 4-12: Responses of the feedback linearization control and the adaptive feedback linearization control with a modeling error (1kg) and no noise to keep the initial angle (90 degree)

4-4 Conclusion

The sliding mode algorithm or the indirect adaptive algorithm has to be added to the feedback linearization method in order to estimate the mass variation of the end-effector. Both algorithms can estimate the mass with good performances in the same conditions. However, the sliding mode algorithm with the feedback linearization method shows smaller tracking error and faster rise time than the performance of the indirect adaptive algorithm as shown in Figure 4.9 and 4.12. Moreover, the process of the sliding mode control is simpler than the indirect adaptive control, which requires least square calculation for parameter estimation. To simulate the overall dynamic model of the link system with hardware saturations, the sliding mode algorithm is applied in next chapter.

Simulation with overall dynamic model

In this chapter, the feedback linearization control with the sliding mode algorithm is implemented for the trajectory tracking of the overall dynamic system of Figure 2.1. The overall dynamic model is used to choose proper gains of the controller of the system considering maximum motor speeds, maximum motor torques, current saturations, and voltage saturations of the macro-micro actuators with parameter values of Table 5.1 and 5.2.

r	0.075[m]	m	0.35[kg]
k	$568[\frac{kg}{s^2}]$	l	0.4[m]

Table 5-1: Parameter values of the manipulator

R_m	21 [ohm]	R_M	0.605 [ohm]
L_m	0.00137 [H]	L_M	0.000191 [H]
J_m	4.13×10^{-7} [kgm ²]	J_M	79.2×10^{-7} [kgm ²]
k_g	410 [-]	k_G	1 [-]
k_b	0.0212 [Vs/rad]	V_B	0.0292 [Vs/rad]
B_m	5.8×10^{-6} [kgm ² /sec]	B_M	5.8×10^{-6} [kgm ² /sec]
k_i	0.0212 [Nm/A]	k_I	0.0292 [Nm/A]
		p	0.00254 [m]

Table 5-2: Parameter values of the macro-micro actuator dynamics

The gains of the PD controller, K_p and K_d , with the sliding constants, λ , were designed to have less than 0.5 degree error following the 3 second cubic polynomial trajectory, avoiding the hardware saturation of Table 5.3. Designed gains of the PD controller and the sliding constants are defined as follows.

$$K_p = \begin{bmatrix} 49 & 0 \\ 0 & 16 \end{bmatrix}, \quad K_d = \begin{bmatrix} 14 & 0 \\ 0 & 8 \end{bmatrix}, \quad \lambda = \begin{bmatrix} 1 \\ 0.1 \end{bmatrix}$$

Figure 5.1 shows the time responses of the single rotating link system based on the above conditions and controllers when the mass of the end-effector is 2kg during the simulation. Current, voltage, maximum continuous torques, and maximum motor speeds of both actuators are within the boundary of the saturations; the peak torque is limited to 4 to 5 times maximum continuous torque [11]. At the initial simulation time, current and voltage of both macro actuator and micro actuator are increased to adapt the mass 2kg. The link tracks the given trajectory with a small error until the macro actuator converges static balance point of the system after small overshoot at the initial time. The sliding mode algorithm estimates the mass 2kg as 1.9kg as shown in Figure 5.2. The 0.1kg estimation error is caused by the trajectory variation. If the trajectory is slower, the error becomes smaller. The estimation error results in the convergence error of the macro actuator. As a result, the system is not in the perfect static balance, but it is reasonable. The trajectory error of the link is about 0.3 degree so that this perfectly satisfies the requirements; the tracking time cannot be less than 3 second because the tracking error becomes over 0.5 degree. These simulation results are visualized by Virtual Reality Modeling Language (VRML) model as shown in Figure 5.3.

The micro actuator factors	saturations	The macro actuator factors	saturations
Max. motor speed	1026 [rad/sec]	Max. motor speed	1256 [rad/sec]
Max. continuous torque	0.00697 [Nm]	Max. continuous torque	0.0933 [Nm]
Voltage	± 27.5 [V]	Voltage	± 27.5 [V]
Current	± 3 [A]	Current	± 3 [A]

Table 5-3: Hardware saturations

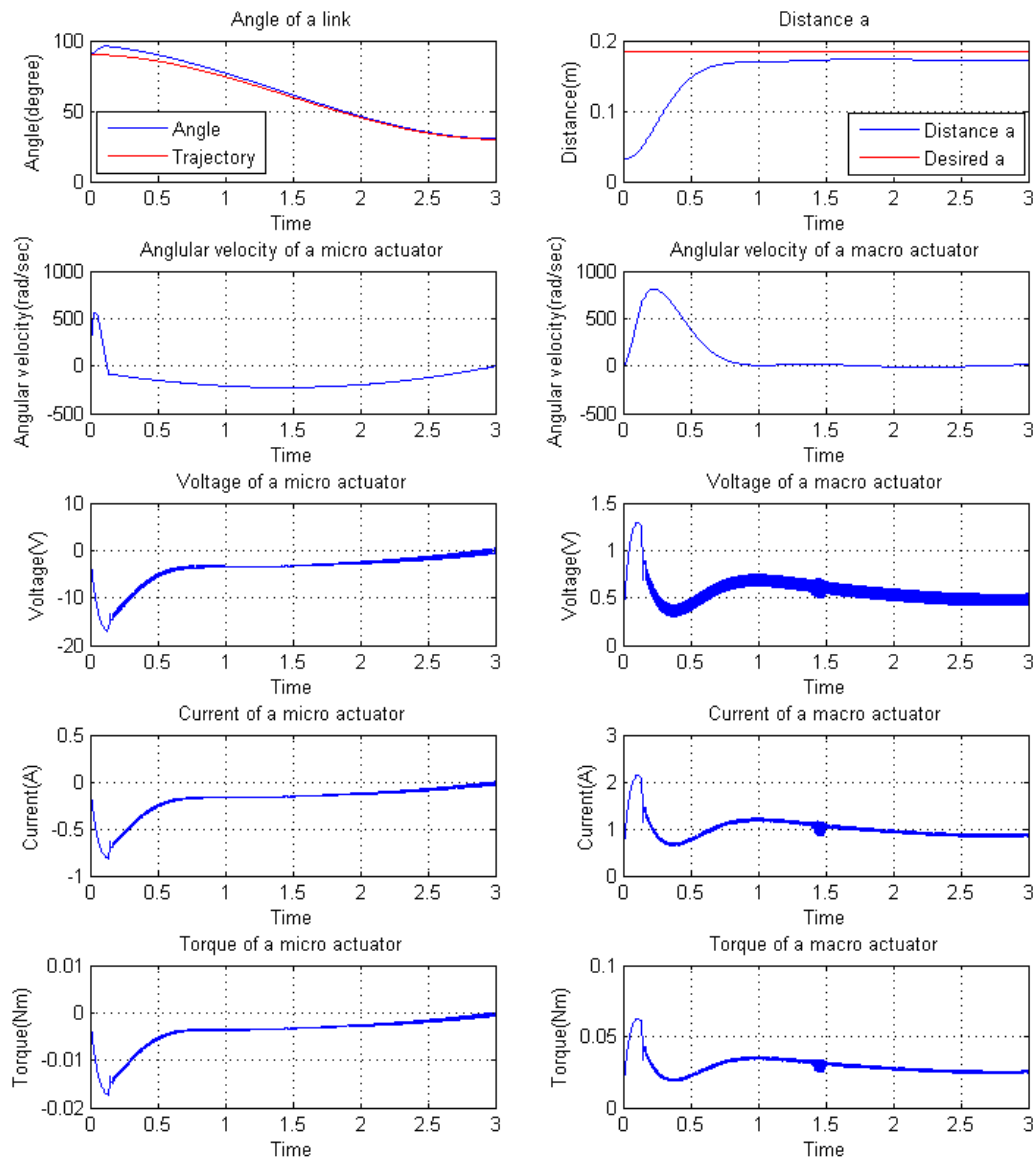


Figure 5-1: Responses of the system with cubic polynomial trajectory input

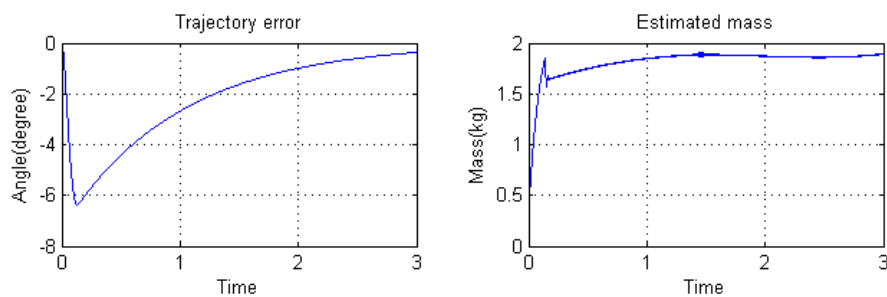


Figure 5-2: Tracking error and Estimation mass

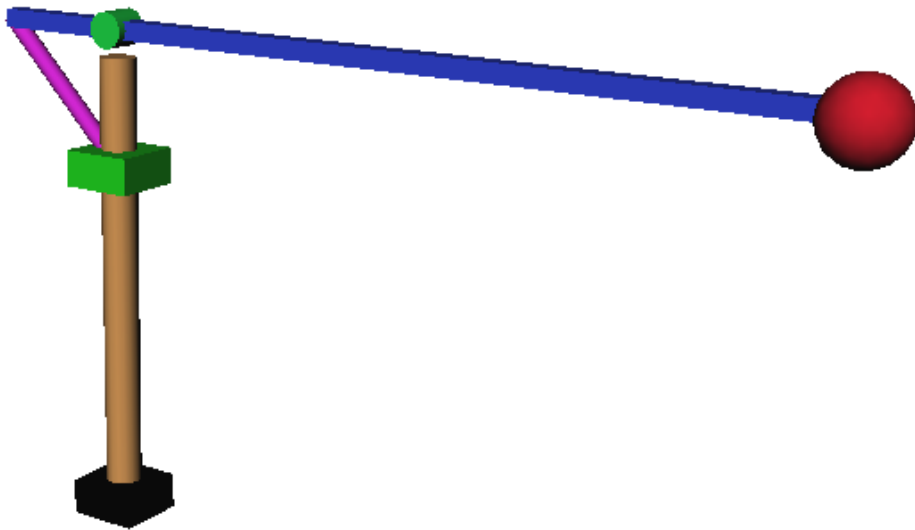


Figure 5-3: 3D Virtual Reality Model of the single rotating link system

Conclusions and Recommendations

6-1 Conclusions

This research aimed at finding the best control scheme with a controller for the macro-micro actuated system of the Delft robot arm and reached the following conclusions based on the problem definitions of Chapter 1.

1. For simulation purpose, a dynamic model of the manipulator and actuator dynamics are successfully derived using the symbolic toolbox of Matlab. In order to understand the motion of the system, the dynamic model was visualized through the Virtual Reality Modeling Language (VRML) by means of a Matlab script which applies the output data and the VRML model in generating a 3D animation.
2. To analyze the system properties, the present study checked the nonlinearity of the system, the influence of an unknown mass attached to the end-effector, the stability of Multi-Input-Multi-Output (MIMO) system, and the performance limitation by hardware saturations in Chapter 3 and Chapter 5. The nonlinearity of the system, resulted from mass and angle, was confirmed by the gain variation of root locus and time response of the closed loop system. The stability of the MIMO system was examined to design controllers by characteristics loci, which uses eigenvalues of the system and Nyquist criterion theorem. Lyapunov direct method was used to check the stability of the feedback linearization control system. However, the stability of non-autonomous system with a linear controller could not be confirmed. The performance limitation by hardware saturations was checked by simulation.
3. The third subgoal was to survey several control schemes with controllers. Three control schemes, Tracking/Compensating mode, Tracking/Tracking mode, Balancing/Tracking mode, were simulated with PID controllers. Tracking/Compensating mode can not have both high bandwidth of the macro actuator and the whole system, but it has adaptivity against the mass variation without any advanced algorithm. Tracking/Tracking mode makes the macro-micro actuators share the tracking work depending on the relative

magnitude of gains of controllers, and results in high torque of the micro actuator since the system does not use the static balancing concept. Balancing/Tracking mode uses two different feedback signal for the macro-micro actuators and makes the system in static balance. However it needs an advanced algorithm, such as a sliding mode algorithm and an indirect adaptive algorithm, to estimate the mass variation of the end-effector.

4. To choose the best control scheme for the macro-micro actuated system, the performance of the system with the control schemes and controllers were compared. The system must have low actuation power of the micro actuator, small position error and high bandwidth performance within the permissible boundaries of motor speeds, motor torques, current, and voltage. To remove the nonlinearity of the system and decouple the MIMO system, a feedback linearization controller was used instead of a linear controller. Balancing/Tracking mode was selected as the best control scheme among the three candidates. It is the best method which showed the lowest actuation power of the micro actuator and high-bandwidth performance of the macro actuator within the range of the hardware saturations as presented in Figure 3.21; the torques of the micro actuator of three control schemes were about 6.6, 6.7, and 6.3 [Nm] respectively. The static balancing concept works only in the Balancing/Tracking mode. To estimate the mass variation, the sliding mode algorithm was selected, since it shows smaller tracking error during the motion and faster rise time than the indirect adaptive algorithm as suggested in Chapter 4; the feedback linearization method with the sliding mode algorithm and the indirect adaptive algorithm were about 0.4 sec. and 0.5 sec. respectively. The chosen control scheme with the advanced algorithm was used to simulate the overall dynamic model of the macro-micro actuated system considering motor speeds, motor torques, current, and voltage. For the fast response and the safety of the single rotating link system, the macro actuator should has high power with high speed and the power of the micro actuator should be as low as possible in the given hardware saturations and limitations.

6-2 Recommendations

- The total simulation model needs verification, because assumptions, i.e. mass, inertia properties, and the center of mass, are made in the modeling of the manipulator. Parameters such as length and other dimensions are derived from the mechanical drawings. To simulate accurately the real system, system identification should be performed. Furthermore, it is recommended to estimate friction with mass of the end-effector since the friction of the system changes depending on the angle and mass of the end-effector.
- The present study assumed the manipulator to be equipped with an angular velocity sensor. If the real system does not have the sensor, the controller of the system has to be designed with observers to estimate the angular velocity.
- The stability of the closed loop system with feedback linearization method can be proven as shown in Chapter 4. However, the stability of the closed loop system with a PID controller was failed to be proven. It could be an interesting work to prove the stability of a non-autonomous system with a linear controller considering its boundary.

- The combination of the model based part and the servo part in a feedback linearization method simplifies the tuning of control gains. It will be another challenge to compare this result with the other control methods such as an adjustable pole placement method, knowledge based control methods, and a passivity based control.
- In this paper, the single rotating link system is used to find a proper control scheme with a controller. The chosen control scheme can be applied to 4DOF Delft robot arm for the future work, using kinematics and dynamics of the Delft robot arm in Appendix D.

Appendix A

Stability Analysis

The closed loop system in Chapter 3, which has mass variation of the end-effector, is a non-autonomous system. It is difficult to check the stability of the non-autonomous system since the system is nonlinear and mass is changed. In this chapter, Lyapunov direct method with sector nonlinearity and vanishing perturbation, are introduced to prove the stability of the non-autonomous system.

A-1 Problem Statement

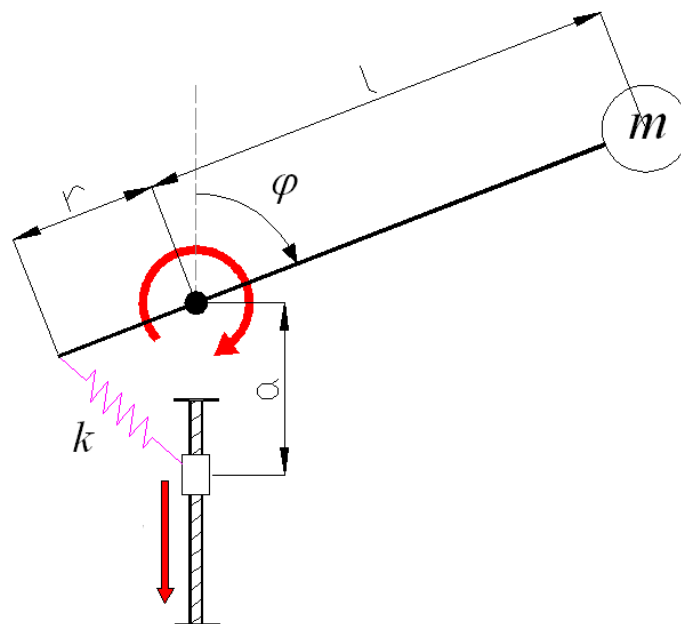


Figure A-1: Diagram of a simplified single rotating link system, The control signal is α

The system can be expressed:

$$\ddot{\varphi}(t) = \sin \varphi(t) \left(\frac{g}{l} - \frac{kr}{l^2 m(t)} a(t) \right)$$

A PID controller and an initial condition is used for a control input, $a(t)$:

$$a(t) = a_0 + k_p(\varphi_r - \varphi(t)) - k_d \dot{\varphi}(t) + k_i \int (\varphi_r - \varphi(t)) dt$$

where a_0 is obtained from the equilibrium condition ($\ddot{\varphi}(t) = 0, \forall t$) for a given mass m_0 :

$$\frac{g}{l} = \frac{kr}{l^2 m_0} a_0 \Rightarrow a_0 = \frac{gl}{kr} m_0$$

The angle $\varphi(t)$ and the mass $m(t)$ vary in a given range, such as 30 to 150 degrees and 0.35 to 2 kg, respectively.

The problems to solve by using nonlinear analysis / synthesis:

1. Check the stability of the closed loop system with a known mass, given the gains k_p , k_i and k_d .
2. Check the stability of the closed loop system with observable varying mass, given the gains k_p , k_i and k_d .
3. Check the stability of the closed loop system with unobservable varying mass, given the gains k_p , k_i and k_d .

In Section A-2 and A-3, the above three problems are checked by using sector nonlinearity and vanishing perturbation.

A-2 Lyapunov direct method with Sector nonlinearity

For the stability analysis of fuzzy systems ($\dot{x}(t) = f(x(t)) = A(t)x(t)$), Tanaka and Sugeno have derived a stability theorem using Lyapunov direct method [12]. In the theorem, an existence of the positive definite matrix P , which is common to the Lyapunov inequalities consisting of linear subsystems, plays an important role.

$$\begin{aligned} V &= x^T P x \\ \dot{V} &= \dot{x}^T P x + x^T P \dot{x} \\ &= (x^T A) P x + x^T P (A x) \\ &= x^T (A^T P + P A) x < 0 \quad \forall x \end{aligned}$$

The linear subsystems of a nonlinear system are derived from sector nonlinearity approach. Figure A.2 illustrates the local sector nonlinearity approach, where two lines become the local sectors under $-d < x(t) < d$. This is reasonable as variables of physical systems are always bounded. From the various bounded variables, the linear subsystems are determined, and

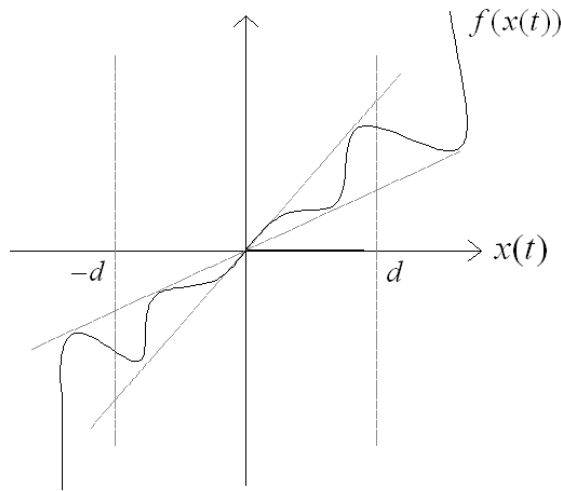


Figure A-2: Sector nonlinearity

the nonlinear system is asymptotically stable in the large if there exists a common positive definite matrix P for all the subsystems such that A_i is stable and nonsingular, and

$$A_i^T P + P A_i < 0 \quad \text{for } \forall i \in 1, 2, \dots$$

This is based on Lyapunov's direct method, and it should be noticed that the theorem gives a sufficient condition for the stability, and a fuzzy system is not always asymptotically stable in the large even if all the A_i 's are stable matrices. Therefore, it is desired to find the common positive definite matrix P in a simple manner.

A-2-1 The sector nonlinearity for a system assuming the system is in perfect static balance

Control input is

$$a(t) = a_0 + k_p(\varphi_r - \varphi(t)) - k_d\dot{\varphi}(t) + k_i \int (\varphi_r - \varphi(t)) dt$$

State definition and state space model of the single rotating link system are expressed as follows.

$$x_1 = \varphi(t) - \varphi_r, \quad x_2 = \dot{x}_1 = \dot{\varphi}(t), \quad x_i = \int x_1 dt$$

$$\dot{x}_1 = x_2$$

$$\dot{x}_2 = \frac{g}{l} \sin \varphi(t) + \frac{-kr}{m_0 l^2} \sin \varphi(t) [a_0 - k_p x_1 - k_d x_2 - k_i x_i] = \frac{-kr}{m_0 l^2} \sin \varphi(t) [-k_p x_1 - k_d x_2 - k_i x_i]$$

$$\dot{x}_i = x_1$$

$$\begin{bmatrix} \dot{x}_1 \\ \dot{x}_2 \\ \dot{x}_i \end{bmatrix} = \begin{bmatrix} 0 & 1 & 0 \\ \frac{krk_p}{m_0 l^2} \sin \varphi(t) & \frac{krk_d}{m_0 l^2} \sin \varphi(t) & \frac{krk_i}{m_0 l^2} \sin \varphi(t) \\ 1 & 0 & 0 \end{bmatrix} \begin{bmatrix} x_1 \\ x_2 \\ x_i \end{bmatrix}$$

Since the operational range of an angle $\varphi(t)$ is from 30 to 150 degree, $\sin \varphi(t)$ is in the below range.

$$\sin \varphi(t) \in \left[\frac{1}{2}, 1\right]$$

Then, two rules are derived from the above range and state space form.

Rule 1: if $\sin \varphi(t)$ is around 0.5,

$$\begin{bmatrix} \dot{x}_1 \\ \dot{x}_2 \\ \dot{x}_i \end{bmatrix} = \begin{bmatrix} 0 & 1 & 0 \\ \frac{krk_1}{2m_0l^2} & \frac{krk_2}{2m_0l^2} & \frac{krk_i}{2m_0l^2} \\ 1 & 0 & 0 \end{bmatrix} \begin{bmatrix} x_1 \\ x_2 \\ x_i \end{bmatrix}$$

Rule 2: if $\sin \varphi(t)$ is around 1,

$$\begin{bmatrix} \dot{x}_1 \\ \dot{x}_2 \\ \dot{x}_i \end{bmatrix} = \begin{bmatrix} 0 & 1 & 0 \\ \frac{krk_1}{m_0l^2} & \frac{krk_2}{m_0l^2} & \frac{krk_i}{m_0l^2} \\ 1 & 0 & 0 \end{bmatrix} \begin{bmatrix} x_1 \\ x_2 \\ x_i \end{bmatrix}$$

The gains of the PID controller ($k_p=-1.2$, $k_d=-1$, $k_i=-1.8$) are designed by a linearized model with Root Locus, and the stability of this closed loop system is checked using Matlab's Linear Matrix Inequality (LMI) Toolbox. The system is stable with the pre-designed controller when the mass is equal to an initial mass since the positive definite matrix, P , exists.

A-2-2 The sector nonlinearity for a system assuming the mass is variable and observable

Control input is

$$a(t) = a_0 + k_p(\varphi_r - \varphi(t)) - k_d\dot{\varphi}(t) + k_i \int (\varphi_r - \varphi(t))dt$$

State definition and state space model of the single rotating link system are expressed as follows.

$$x_1 = \varphi(t) - \varphi_r, \quad x_2 = \dot{x}_1 = \dot{\varphi}(t), \quad x_i = \int x_1 dt$$

$$\dot{x}_1 = x_2$$

$$\dot{x}_2 = \frac{g}{l} \sin \varphi(t) - \frac{kr}{m(t)l^2} \sin \varphi(t) [a_0 - k_p x_1 - k_d x_2 - k_i x_i]$$

$$\dot{x}_i = x_1$$

$$\begin{bmatrix} \dot{x}_1 \\ \dot{x}_2 \\ \dot{x}_i \end{bmatrix} = \begin{bmatrix} 0 & 1 & 0 \\ \frac{krk_p}{m(t)l^2} \sin \varphi(t) & \frac{krk_d}{m(t)l^2} \sin \varphi(t) & \frac{krk_i}{m(t)l^2} \sin \varphi(t) \\ 1 & 0 & 0 \end{bmatrix} \begin{bmatrix} x_1 \\ x_2 \\ x_i \end{bmatrix} + \begin{bmatrix} 0 \\ (\frac{g}{l} - \frac{kr}{m(t)l^2} a_0) \sin \varphi(t) \\ 0 \end{bmatrix} \quad (\text{A-1})$$

Since the operational range of an angle $\varphi(t)$ is from 30 to 150 degree and $m(t)$ is variable between 0.35kg and 2kg, $\frac{\sin \varphi(t)}{m(t)}$ is in the below range.

$$\frac{\sin \varphi(t)}{m(t)} \in \left[\frac{1}{4}, \frac{100}{35}\right]$$

Assuming that the mass can be observed, $a_0 = \frac{m(t)gl}{kr}$ and the state space description is

$$\begin{bmatrix} \dot{x}_1 \\ \dot{x}_2 \\ \dot{x}_i \end{bmatrix} = \begin{bmatrix} 0 & 1 & 0 \\ \frac{krk_p}{m(t)l^2} \sin \varphi(t) & \frac{krk_d}{m(t)l^2} \sin \varphi(t) & \frac{krk_i}{m(t)l^2} \sin \varphi(t) \\ 1 & 0 & 0 \end{bmatrix} \begin{bmatrix} x_1 \\ x_2 \\ x_i \end{bmatrix}$$

Then, the below two rules are derived from the above state space form.

Rule 1: if $\frac{\sin \varphi(t)}{m(t)}$ is around $\frac{1}{4}$,

$$\begin{bmatrix} \dot{x}_1 \\ \dot{x}_2 \\ \dot{x}_i \end{bmatrix} = \begin{bmatrix} 0 & 1 & 0 \\ \frac{krk_p}{4l^2} & \frac{krk_d}{4l^2} & \frac{krk_i}{4l^2} \\ 1 & 0 & 0 \end{bmatrix} \begin{bmatrix} x_1 \\ x_2 \\ x_i \end{bmatrix}$$

Rule 2: if $\frac{\sin \varphi(t)}{m(t)}$ is around $\frac{100}{35}$,

$$\begin{bmatrix} \dot{x}_1 \\ \dot{x}_2 \\ \dot{x}_i \end{bmatrix} = \begin{bmatrix} 0 & 1 & 0 \\ \frac{100krk_p}{35l^2} & \frac{100krk_d}{35l^2} & \frac{100krk_i}{35l^2} \\ 1 & 0 & 0 \end{bmatrix} \begin{bmatrix} x_1 \\ x_2 \\ x_i \end{bmatrix}$$

The gains of the PID controller (kp=-1.2, kd=-1, ki=-1.8) are designed by a linearized model with Root Locus, and the stability of this closed loop system is checked by LMI method. The system is stable with the pre-designed controller when the mass is variable and observable.

A-2-3 The sector nonlinearity for a system assuming the mass is variable, but unobservable

If the mass is not observed, affine models are obtained from the equation A-1 and expressed in the below two rules. Then, this model does not guarantee the stability of a system.

Rule 1: if $\frac{\sin \varphi(t)}{m(t)}$ is around $\frac{1}{4}$,

$$\begin{bmatrix} \dot{x}_1 \\ \dot{x}_2 \\ \dot{x}_i \end{bmatrix} = \begin{bmatrix} 0 & 1 & 0 \\ \frac{krk_p}{4l^2} & \frac{krk_d}{4l^2} & \frac{krk_i}{4l^2} \\ 1 & 0 & 0 \end{bmatrix} \begin{bmatrix} x_1 \\ x_2 \\ x_i \end{bmatrix} + \begin{bmatrix} 0 \\ \frac{g}{2l} - \frac{g}{4l}m_0 \\ 0 \end{bmatrix}$$

Rule 2: if $\frac{\sin \varphi(t)}{m(t)}$ is around $\frac{100}{35}$,

$$\begin{bmatrix} \dot{x}_1 \\ \dot{x}_2 \\ \dot{x}_i \end{bmatrix} = \begin{bmatrix} 0 & 1 & 0 \\ \frac{100krk_p}{35l^2} & \frac{100krk_d}{35l^2} & \frac{100krk_i}{35l^2} \\ 1 & 0 & 0 \end{bmatrix} \begin{bmatrix} x_1 \\ x_2 \\ x_i \end{bmatrix} + \begin{bmatrix} 0 \\ \frac{g}{l} - \frac{100g}{35l}m_0 \\ 0 \end{bmatrix}$$

A-3 Vanishing Perturbation

Sector nonlinearity cannot prove the stability of the closed loop system which has the affine model. In this section, an another method, vanishing perturbation, is tried to check the stability. The vanishing perturbation uses concept of robustness based on the below Lemma [13].

Lemma If the origin is exponentially stable equilibrium of the nominal system $\dot{x} = f(t, x)$, then the origin will be exponentially stable equilibrium also for the perturbed system $\dot{x} = f(t, x) + g(t, x)$ under following conditions.

The perturbation term satisfies the linear growth bound:

$$\begin{aligned} \|g(t, x)\| &\leq \gamma \|x\| \\ 0 < \gamma &\leq \frac{C_3}{C_4} \end{aligned}$$

where C_3 and C_4 are determined from below conditions that will assure exponential stability of the system:

$$\begin{aligned} C_1 \|x\|^2 &\leq V(t, x) \leq C_2 \|x\|^2 & (A-2) \\ \lambda_{\min}(P) \|x\|_2^2 &\leq x^T P x \leq \lambda_{\max}(P) \|x\|_2^2 \\ C_1 &= \lambda_{\min}(P), \quad C_2 = \lambda_{\max}(P) \end{aligned}$$

where λ is eigenvalue.

$$\frac{\partial V}{\partial t} + \frac{\partial V}{\partial x} f(t, x) \leq -C_3 \|x\|^2 \quad (A-3)$$

$$\begin{aligned} \dot{V} &= \dot{x}^T P x + x^T P \dot{x} = f(t, x)^T P x + x^T P f(t, x) \\ &= x^T A^T P x + x^T P A x = x^T (A^T P + P A) x \end{aligned}$$

since $PA + A^T P = -I$

$$\begin{aligned} \dot{V} &\leq -\|x\|_2^2 \\ -\lambda_{\max}(I) \|x\|_2^2 &\leq \frac{\partial V}{\partial x} f(t, x) = -x^T x \leq -\lambda_{\min}(I) \|x\|_2^2 \\ C_3 &= \lambda_{\min}(I) = 1 \end{aligned}$$

$$\left\| \frac{\partial V}{\partial x} \right\| \leq C_4 \|x\| \quad (A-4)$$

$$\begin{aligned} V(x) &= x^T P x \leq \|x\|_2^2 \|P\| \\ \left\| \frac{\partial V}{\partial x} \right\|_2 &= \|2x^T P\|_2 \leq 2\|P\|_2 \|x\|_2 = 2\lambda_{\max}(P) \|x\|_2 \\ C_4 &= 2\lambda_{\max}(P) \end{aligned}$$

The derivative of Lyapunov function, V , along the trajectories of perturbed system is expressed using the above conditions.

$$\dot{V}(t, x) = \frac{\partial V}{\partial t} + \frac{\partial V}{\partial x} f(t, x) + \frac{\partial V}{\partial x} g(t, x)$$

$$\dot{V} \leq -C_3 \|x\|^2 + \frac{\partial V}{\partial x} g(t, x) \leq -C_3 \|x\|^2 + C_4 \|x\| \|g(t, x)\| \leq -C_3 \|x\|^2 + C_4 \|x\| \gamma \|x\|$$

Since the growth bound is only information on $g(t, x)$, a conservative approach is taken to estimate the region of attraction:

$$\begin{aligned}\dot{V} &\leq -C_3\|x\|^2 + C_4\|x\|\gamma\|x\| \leq 0 \\ C_4\|x\|\gamma\|x\| &< C_3\|x\|^2 \quad \Rightarrow \quad \gamma < \frac{C_3}{C_4}\end{aligned}$$

The above vanishing perturbation theory is used to check the stability of the single rotating link system. The state space of (A-1) except an integral controller can be expressed as follow.

$$\dot{x} = f(t, x) + g(t, x)$$

$$\begin{bmatrix} \dot{x}_1 \\ \dot{x}_2 \end{bmatrix} = \begin{bmatrix} 0 & 1 \\ \frac{krk_p}{m(t)l^2} \sin \varphi(t) & \frac{krk_d}{m(t)l^2} \sin \varphi(t) \end{bmatrix} \begin{bmatrix} x_1 \\ x_2 \end{bmatrix} + \begin{bmatrix} 0 \\ (\frac{g}{l} - \frac{kr}{m(t)l^2}a_0) \sin \varphi(t) \end{bmatrix}$$

Matrix $f(t, x)$ is assumed that the nominal system is in the worst case: $m(t) = 2$ and $\varphi(t) = \frac{\pi}{6}$. k_p and k_d are assumed as -0.2 and -0.2. Then, the system is expressed as

$$\begin{aligned}\dot{x} &= f(t, x) + g(t, x) = Ax + g(t, x) \\ &= \begin{bmatrix} 0 & 1 \\ -13 & -13 \end{bmatrix} x + \begin{bmatrix} 0 \\ (\frac{g}{l} - \frac{kr}{m(t)l^2}a_0) \sin \varphi(t) \end{bmatrix}\end{aligned}$$

The solution of the Lyapunov equation:

$$PA + A^T P = -I$$

is given by:

$$P = \begin{bmatrix} 1.0197 & 0.0188 \\ 0.0188 & 0.0195 \end{bmatrix}$$

$V(x) = x^T P x$ satisfies the below inequalities:

- (1) $C_1\|x\|^2 \leq V(t, x) \leq C_2\|x\|^2$ where $C_1 = \lambda_{\min}(P) = 0.0191$ and $C_2 = \lambda_{\max}(P) = 1.0201$
- (2) $\frac{\partial V}{\partial t} + \frac{\partial V}{\partial x} f(t, x) \leq -C_3\|x\|^2$ where $C_3 = \lambda_{\min}(I) = 1$
- (3) $\|\frac{\partial V}{\partial x}\| \leq C_4\|x\|$ where $C_4 = 2\lambda_{\max}(P) = 2.0402$
- (4) $\|g(t, x)\| \leq \gamma\|x\|^2$

taking $|x_1| \geq \alpha$:

$$\|g(x)\|_2 \leq \frac{\beta}{\alpha}|x_1| \leq \gamma\|x_1\|_2$$

where $\gamma = \frac{\beta}{\alpha}$, $\beta = \frac{g}{l} \sin \varphi(t)(1 - \frac{m_0}{m(t)})$, and $\alpha = \pi/6$ (the smallest angle)

Taking Lyapunov function:

$$\dot{V} \leq -C_3\|x\|^2 + \frac{\partial V}{\partial x} g(t, x) = -C_3\|x\|^2 + C_4\|x\|\gamma\|x\|$$

Substituting C_3, C_4 , and γ :

$$\dot{V} \leq -\|x\|^2 + 2.0402 \frac{6}{\pi} \beta \|x\|^2$$

$\dot{V} < 0$ if $-||x||^2 + 2.0402\frac{6}{\pi}\beta||x||^2 < 0$, hence:

$$\beta < \frac{\pi}{2.0402 \times 6}$$

$$\beta = \frac{g}{l} \sin \varphi(t) \left(1 - \frac{m_0}{m(t)}\right) = \frac{9.81}{0.4} \left(1 - \frac{0.35}{m(t)}\right) < \frac{\pi}{2.0402 \times 6} \Rightarrow m(t) < 0.3537$$

The maximum mass is 0.3537kg for the stability of a system. However, the same controller can make a system stable with 3kg mass in simulation. This method does not show anything about stability.

Appendix B

PID cascade control

In Chapter 3, the mass of the leadscrew nut or the rotor inertia of the macro actuator were not included in motion equations. This provides a simple calculation to design a controller in the three control schemes. However, such designed controller cannot be implemented in Tracking/Compensating mode and Tracking/Tracking mode when the mass of the lead screw nut or the rotor inertia of the macro actuator are considered, since the closed loop system becomes fourth order system having only one zero.

Considering the mass of the leadscrew nut or the rotor inertia of the macro actuator, the motion equations are expressed as follows; where m_a is the mass of the leadscrew nut or rotor inertia of the actuator.

$$\begin{aligned} ml^2\ddot{\varphi} + (kar - mgl) \sin \varphi &= \tau \\ m_a\ddot{a} - m_ag + ka - kr \cos \varphi &= F \end{aligned}$$

Linearizing the nonlinear equations,

$$\begin{cases} ml^2\ddot{\varphi} + kar \sin \varphi_e = \tau \\ m_a\ddot{a} + ka + kr \sin \varphi_e \varphi = F \end{cases} \quad (\text{B-1})$$

It is assumed that τ equals zero and the macro actuator is used to control angle φ . Then, the transfer function of $\frac{\varphi(s)}{F(s)}$ is expressed as below.

$$G(s) = \frac{\varphi(s)}{F(s)} = \frac{-A}{m_a ml^2 s^4 + km l^2 s^2 - A^2} \quad \text{where } A = kr \sin \varphi_e$$

A PD controller ($H(s) = k_d s + k_p$) is considered to control this system.

$$G(s)H(s) = \frac{k_p(-qs - 1)(-A)}{m_a ml^2 s^4 + km l^2 s^2 - A^2} \quad \text{where } q = \frac{k_d}{k_p} = 0.3$$

However, it is impossible to design the PD controller as shown in Root Locus plot of $G(s)H(s)$ of Figure B.1. A stable system must have all its closed loop poles in LHP.

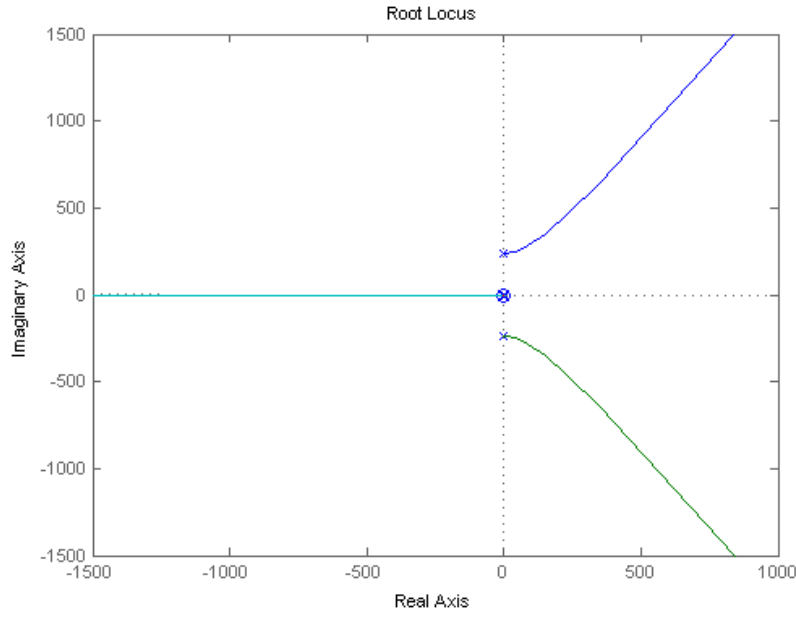


Figure B-1: Root Locus of $G(s)H(s)$

Thus, a PID cascade controller has to be considered instead of the PD controller for the macro actuator as shown in Figure B.2. First, an inner PD controller for $\frac{a(s)}{F(s)}$ is designed. Assuming the spring force as a disturbance, the inner PD controller ($k_{d1}s + k_{p1}$) for $\frac{a(s)}{F(s)}$ can be designed as $7(0.3s+1)$ with the below transfer function.

$$\frac{a(s)}{F(s)} = \frac{1}{m_a s^2 + k}$$

An outer PID controller is designed with the below transfer function, which considers the spring force with the inner closed loop system.

$$\frac{\varphi(s)}{x(s)} = \frac{-A(k_{d1}s + k_{p1})}{m_a m l^2 s^4 + m l^2 k_{d1} s^3 + (k + k_{p1}) m l^2 s^2 - A^2}$$

The outer PID controller is designed as $-6(s^2 + 2s + 1)$. As shown in Figure B.3, this PID cascade controller works with the original nonlinear system. The responses of the closed loop system of the linearized model and the original nonlinear model are similar and the macro actuator moves the leadscrew nut to the static balancing point without any observers.

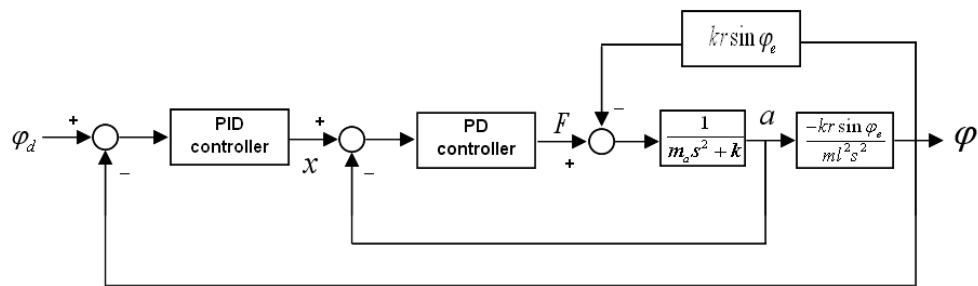


Figure B-2: Block diagram of the PID cascade controller

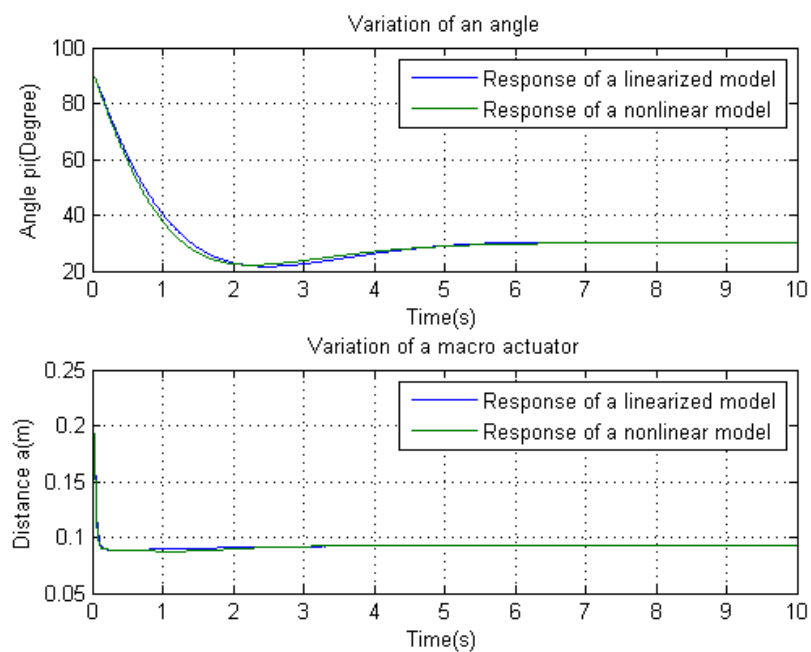


Figure B-3: Responses of the linearized system and the original nonlinear system with the PID cascade controller

Cubic polynomial trajectory

A trajectory planner can decrease the initial load of the actuator such as the initial surge torque and the initial surge voltage generated by the step input in Chapter 3. One of the trajectory planner is a cubic polynomial trajectory planner. Changing a desired input gradually depending on time (t), the cubic polynomial trajectory planner produces a single smooth trajectory as shown in Figure C.1.

At least four constraints on $\varphi(t)$ requires to make a single smooth motion. Two constraints on the function's value come from the selection of initial (φ_0) and final values (φ_f) [14]: where t_f is a final time.

$$\varphi(0) = \varphi_0$$

$$\varphi(t_f) = \varphi_f$$

An additional two constraints are that the function be continuous in velocity, which in this case means that the initial and final velocity are known.

$$\dot{\varphi}(0) = \dot{\varphi}_0$$

$$\dot{\varphi}(t_f) = \dot{\varphi}_f$$

These four constraints can be satisfied by a polynomial of at least third degree. These constraints uniquely specify a particular cubic. A cubic has the form

$$\varphi(t) = a_0 + a_1t + a_2t^2 + a_3t^3 \tag{C-1}$$

so the joint velocity and acceleration along this path are clearly

$$\dot{\varphi}(t) = a_1 + 2a_2t + 3a_3t^2 \tag{C-2}$$

$$\ddot{\varphi}(t) = 2a_2 + 6a_3t \tag{C-3}$$

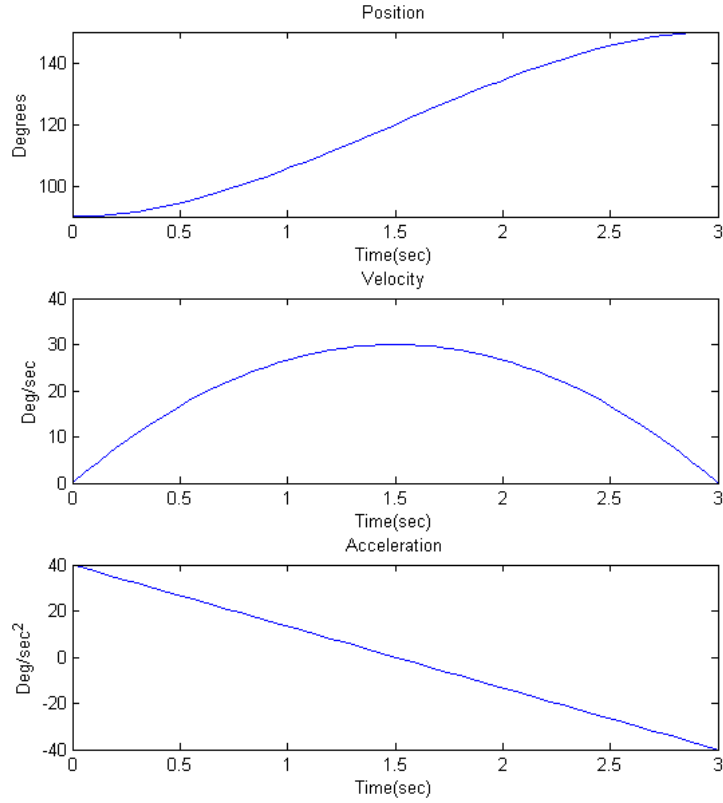


Figure C-1: Position, velocity, and acceleration profiles for a single cubic segment that starts and ends at rest

Combining (C.1) and (C.2) with the four desired constraints yields four equations in four unknowns:

$$\varphi_0 = a_0 \quad (\text{C-4})$$

$$\varphi_f = a_0 + a_1 t_f + a_2 t_f^2 + a_3 t_f^3 \quad (\text{C-5})$$

$$\dot{\varphi}_0 = a_1 \quad (\text{C-6})$$

$$\dot{\varphi}_f = a_1 + 2a_2 t_f + 3a_3 t_f^2 \quad (\text{C-7})$$

Solving these equations for the a_i ,

$$a_0 = \varphi_0 \quad (\text{C-8})$$

$$a_1 = \dot{\varphi}_0 \quad (\text{C-9})$$

$$a_2 = \frac{3}{t_f^2}(\varphi_f - \varphi_0) - \frac{2}{t_f}\dot{\varphi}_0 - \frac{1}{t_f}\dot{\varphi}_f \quad (\text{C-10})$$

$$a_3 = -\frac{2}{t_f^3}(\varphi_f - \varphi_0) + \frac{1}{t_f^2}(\dot{\varphi}_f + \dot{\varphi}_0) \quad (\text{C-11})$$

Using equation C-4, the cubic polynomial that connects any initial and final positions with any initial and final velocities, can be calculated.

Appendix D

Dynamics of a Delft robot arm

In Chapter 2, the mathematical model of the single rotating link system was derived. This model was used to find a proper controller for the macro-micro actuated system in this report. Motion equations of 4 DOF Delft robot arm have to be derived to implement the chosen controller to the Delft robot arm. In this chapter, manipulator dynamics of the Delft robot arm are introduced.

D-1 Kinematics

A convenient configuration is chosen for 4 DOF Delft robot arm, corresponding with zero initial joint angles as shown in Figure D.1. In this configuration, all the joint axes of rotations are exactly aligned with one of the axes of the global Cartesian coordinate system. Local coordinate systems for each of the bodies are located in the center of mass, such that the y-axis is always in the longitudinal direction of the body. Positive directions for the joint rotations of the local axes with respect to the global axes follow from standard conventions. Multiplications of rotation matrices serve to express configurations of the rigid bodies. The body coordinates in space(x_j) can be expressed as the joint angles and the distances of lead nuts (q_j). The equations is given in $x_i = x_i(q_j)$ as shown in equation D-1. The vector of global body coordinate is given as follows; X_i and Φ_i mean the Cartesian coordinate of the link i and the global angle of the link i respectively, and L_{c-i} means the center of mass of L_i .

$$x_i = [X_{34} \quad \Phi_{34} \quad X_{m4} \quad \Phi_{m4} \quad X_{b3} \quad \Phi_{b3} \quad X_{ab} \quad \Phi_{ab} \quad X_{a4} \quad \Phi_{a4} \quad X_m \quad \Phi_m \quad a_2 \quad a_4]^T$$

$$X = [x \quad y \quad z]^T$$

$$\Phi = [\phi_1 \quad \phi_2 \quad \phi_3]^T$$

The vector of generalized coordinates is given:

$$q_j = [\varphi_1 \quad \varphi_2 \quad \varphi_3 \quad \varphi_4 \quad a_2 \quad a_4]^T$$

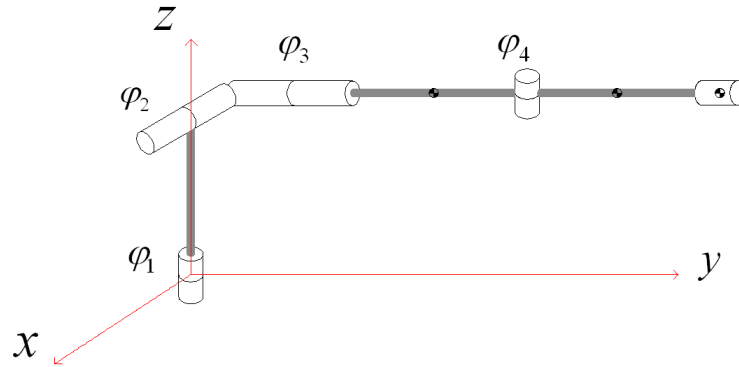


Figure D-1: A schematic diagram of the robot arm model in initial configuration; some of the rigid bodies are not shown. In this configuration, all cylindrical bodies are aligned with the y-axis. For the detail schematic diagram, refer the figure 1.2 and 1.3 in chapter 1

$$\begin{bmatrix} X_{34} \\ \Phi_{34} \\ X_{m4} \\ \Phi_{m4} \\ X_{b3} \\ \Phi_{b3} \\ X_{ab} \\ \Phi_{ab} \\ X_{a4} \\ \Phi_{a4} \\ X_m \\ \Phi_m \\ a_1 \\ a_2 \end{bmatrix} = \begin{bmatrix} R_{123} \begin{bmatrix} 0 \\ L_{c-34} \\ 0 \end{bmatrix} \\ \begin{bmatrix} 0 \\ 0 \\ \varphi_1 \end{bmatrix} + R_{123} \begin{bmatrix} \varphi_2 \\ 0 \\ 0 \end{bmatrix} + R_{123} \begin{bmatrix} 0 \\ \varphi_3 \\ 0 \end{bmatrix} \\ R_{123} \begin{bmatrix} 0 \\ L_{34} \\ 0 \end{bmatrix} + R_{1234} \begin{bmatrix} 0 \\ L_{c-m4} \\ 0 \end{bmatrix} \\ \varphi_3 + R_{123} \begin{bmatrix} 0 \\ 0 \\ \varphi_4 \end{bmatrix} \\ R_{1234} \begin{bmatrix} 0 \\ L_{c-b3} \\ 0 \end{bmatrix} \\ \Phi_4 \\ R_{123} \begin{bmatrix} 0 \\ L_{c-ab} \\ 0 \end{bmatrix} + R_{1234} \begin{bmatrix} 0 \\ L_{b3} \\ 0 \end{bmatrix} \\ R_{1234} \begin{bmatrix} 0 \\ -L_{b3} + L_{c-a4} \\ 0 \end{bmatrix} + R_{123} \begin{bmatrix} 0 \\ L_{ab} \\ 0 \end{bmatrix} \\ \Phi_4 \\ R_{123} \begin{bmatrix} 0 \\ L_{34} \\ 0 \end{bmatrix} + R_{1234} \begin{bmatrix} 0 \\ L_{m4} \\ 0 \end{bmatrix} \\ \Phi_4 \\ a_2 \\ a_4 \end{bmatrix} \quad (D-1)$$

The indices for the rotation matrices in equation D-1 denote subsequent multiplications, such as following equations.

$$R_{12} = R_1 R_2$$

The rotation matrices (R_i) can be expressed using R_x , R_y , and R_z and the joint angles corresponding to Figure D.1.

$$R_1 = R_z(\varphi_1) = \begin{bmatrix} \cos\varphi_1 & -\sin\varphi_1 & 0 \\ \sin\varphi_1 & \cos\varphi_1 & 0 \\ 0 & 0 & 1 \end{bmatrix}$$

$$R_2 = R_x(\varphi_2) = \begin{bmatrix} 1 & 0 & 0 \\ 0 & \cos\varphi_2 & -\sin\varphi_2 \\ 0 & \sin\varphi_2 & \cos\varphi_2 \end{bmatrix}$$

$$R_3 = R_y(\varphi_3) = \begin{bmatrix} \cos\varphi_3 & 0 & \sin\varphi_3 \\ 0 & 1 & 0 \\ -\sin\varphi_3 & 0 & \cos\varphi_3 \end{bmatrix}$$

$$R_4 = R_z(\varphi_4) = \begin{bmatrix} \cos\varphi_4 & -\sin\varphi_4 & 0 \\ \sin\varphi_4 & \cos\varphi_4 & 0 \\ 0 & 0 & 1 \end{bmatrix}$$

D-2 Dynamics

The next step is deriving the differential equations of motion with the mass matrix and external forces. Local coordinate systems for the rigid bodies are related to a global coordinate system in the equation D-1. The local coordinate systems have been chosen along a convenient axis of the rigid bodies, so that the local mass matrices are diagonal. The inertia tensor for the cylindrical bodies is given as follows. The inertia terms I_L are associated with rotation around a longitudinal axis through the center of mass of the long cylindrical body, while I_R is associated with rotation around a radial axis through the center of mass.

$$\begin{bmatrix} I_{xx} & I_{xy} & I_{xz} \\ I_{yx} & I_{yy} & I_{yz} \\ I_{zx} & I_{zy} & I_{zz} \end{bmatrix} = \begin{bmatrix} I_R & 0 & 0 \\ 0 & I_L & 0 \\ 0 & 0 & I_R \end{bmatrix}$$

The complete mass matrix of the system is a diagonal matrix of 38×38 . This matrix corresponds with the vector of X_i of equation D-1. The elements on the diagonal of this mass matrix are as below; M_i and I_i are mass and inertia of the link L_i

$$M = [M_{34} \quad I_{34} \quad M_{m4} \quad I_{m4} \quad M_{b3} \quad I_{b3} \quad M_{ab} \quad I_{ab} \quad M_{a4} \quad I_{a4} \quad M_m \quad I_m \quad m_{a2} \quad m_{a4}]$$

$$M_i = [m_i \quad m_i \quad m_i]$$

$$I = [I_R \quad I_L \quad I_R]$$

The equations of motion for the rigid masses are derived by Lagrangian and Euler angle, and those are often expressed in the joint coordinates; $\bar{M}(\varphi)$ and $\bar{C}(\varphi, \dot{\varphi})\dot{\varphi} + \bar{G}(\varphi)$ are the reduce mass matrix and the reduced force vectors.

$$\tau = \bar{M}(q)\ddot{q} + \bar{C}(q, \dot{q})\dot{q} + \bar{G}(q)$$

The transformations between joint space and Cartesian space can also be made explicit, by using the Jacobian matrix that contains all partial derivatives $T_j = \frac{\partial x_i}{\partial q_j}(q)$ [15, 16, 17]. F_i is gravity force of the link L_i , and m_{a2} and m_{a4} are mass of the two lead nuts.

$$\tau = T_j^T M T_j \ddot{q} + T_j^T M \frac{\partial(T_j \dot{q})}{\partial q} \dot{q} + T_j^T f \quad (\text{D-2})$$

$$\begin{aligned} \tau &= [\tau_1 \quad \tau_2 \quad \tau_3 \quad \tau_4 \quad f_{a2} \quad f_{a4}] \\ f &= [F_{34} \quad I_0 \quad F_{m4} \quad I_0 \quad F_{b3} \quad I_0 \quad F_{ab} \quad I_0 \quad F_{a4} \quad I_0 \quad F_m \quad I_0 \quad -m_{a2}g \quad -m_{a4}g] \\ F_i &= [0 \quad 0 \quad -m_i g] \\ I_0 &= [0 \quad 0 \quad 0] \end{aligned}$$

Since there are springs in the manipulator of the robot arm, the spring element is added in the above motion equations. The relative displacement of the spring element is expressed in terms of the independent generalize coordinates as $D_v(q_i)$. k_i is the spring coefficient, and y'_{si} is the position of spring-end, which is connected to a link. z_{ai} is the position of the lead nut in global coordinate.

$$\tau = T_j^T M T_j \ddot{q} + T_j^T M \frac{\partial(T_j \dot{q})}{\partial q} \dot{q} + T_j^T f + T_j^T D_{vi} \sigma \quad (\text{D-3})$$

$$\begin{aligned} D_{vi} &= \frac{\partial D_v}{\partial q_i} \\ \sigma = D_v k &= \begin{bmatrix} 0 \\ 0 \\ 0 \\ 0 \\ k_1 \sqrt{x_{s1}^2 + y_{s1}^2 + (z_{s1} - z_{a2})^2} \\ k_2 \sqrt{x_{s2}^2 + y_{s2}^2 + (z_{s2} - z_{a4})^2} \end{bmatrix} \\ \begin{bmatrix} x_{s1} \\ y_{s1} \\ z_{s1} \end{bmatrix} &= R_2 \begin{bmatrix} 0 \\ y'_{s1} \\ 0 \end{bmatrix} \\ \begin{bmatrix} x_{s2} \\ y_{s2} \\ z_{s2} \end{bmatrix} &= R_2 R_3 R_4 \begin{bmatrix} 0 \\ y'_{s2} \\ 0 \end{bmatrix} \end{aligned}$$

For the completed model, a diagonal inertia matrix ($M_{actuator}$) containing all actuator and gearbox inertia is taken into account in the motion equations of the robot arm structure as follows.

$$\tau = (T_j^T M T_j + M_{actuator})\ddot{q} + T_j^T M \frac{\partial(T_j \dot{q})}{\partial q} \dot{q} + T_j^T f + T_j^T D_{vi} \sigma \quad (\text{D-4})$$

Bibliography

- [1] M. Zinn and O. Khatib, "A new actuation approach for human friendly robot design," 2002.
- [2] G. Pratt and M. Williamson, "Series elastic actuators," *IEEE*, vol. 1, pp. 399–406, 1995.
- [3] M. Zinn and O. Khatib, "Actuation methods for human-centered robotics and associated control challenges," *Springer-Verlag*, 2003.
- [4] M. Vermeulen and M. Wisse, "Intrinsically safe, yet industrially applicable robot arm; adjustable static balancing and low power actuation." TU Delft.
- [5] G. J. M. Tuijthof and J. L. Herder, "Design, actuation and control of an anthropomorphic robot arm," *Mechanism and Machine Theory*, pp. 945–962, 2000.
- [6] K. Ogata, *System dynamics*. Prentice Hall, 1998.
- [7] S. Skogestad and I. Postlethwaite, *Multivariable feedback control*. John Willey and Sons, 2005.
- [8] M. W. Spong, *Robot modeling and control*. Wiley, 2006.
- [9] E. Slotine and W. Li, *Applied nonlinear control*. Prentice hall, 1991.
- [10] K. J. Astrom and B. Wittenmark, *Adaptive control*. Addison-Wesley publishing company, 1989.
- [11] H. A. Toliyat and G. B. Kliman, *Handbook of electric motors*. Marcel Dekker, Inc., 2004.
- [12] K. Tanaka and H. O. Wang, *Fuzzy control systems design and analysis*. New York: Wiley-Interscience, 2001.
- [13] H. K. Khalil, *Nonlinear systems*. Prentice Hall, 2002.
- [14] J. J. Craig, *Introduction to Robotics*. Prentice Hall, 2005.

-
- [15] R. Q. van der Linde and A. L. Schwab, *Lecture notes of multibody dynamics (wb1413)*. Delft univ. of Tech., 2009.
 - [16] A. A. Shabana, *Dynamics of multibody systems*. Cambridge University Press, 1998.
 - [17] F. C. Moon, *Applied dynamics*. Wiley-VCH, 2008.

Glossary

List of Acronyms

SEA	Series Elastic Actuation
MIMO	Multi-Input-Multi-Output
DOF	Degrees of Freedom
cpt	counts per turn
DAEs	Differential Algebraic Equations
LHP	left half plane
LQR	Linear Quadratic Regulator
RHP	right half plane
VRML	Virtual Reality Modeling Language
LMI	Linear Matrix Inequality

List of Symbols

α	Angle of the lead screw
β	Angle of the micro actuator
ϵ	Prediction error
\hat{C}	Estimates of C
\hat{G}	Estimates of G
\hat{M}	Estimates of M
\hat{m}	Estimate of mass of the end-effector
\hat{V}	Estimate of control input V

λ	Strict positive constant in the sliding mode algorithm
Φ_i	Global angle of the link i
τ_M	Torque of the macro actuator
τ_m	Torque of the micro actuator
θ	Angle of the macro actuator
φ	Angle of the link
φ_d	Desired angle of the link
φ_e	Equilibrium angle of the link
φ_i	Rotation joints of the Delft robot arm
a	Distance of the lead nut
a_e	Equilibrium distance of the lead nut
a_i	Translation joints of the Delft robot arm
B_M	Viscous damping of the macro actuator
B_m	Viscous damping of the micro actuator
C	The vector of Coriolis and centrifugal torques
$C_M(s)$	Controller of the macro actuator
$C_m(s)$	Controller of the micro actuator
D	Dissipation energy
$e(t)$	Tracking error
F_i	Gravity force of the link L_i
G	The vector of gravitational torques
$H(s)$	Low pass filter
I_i	Inertia of the link L_i
I_L	Inertia in a longitudinal direction
I_M	Current of the macro actuator
I_m	Current of the micro actuator
I_R	Inertia in a radial axis
J_M	Rotor inertia of the macro actuator
J_m	Rotor inertia of the micro actuator
k	Spring coefficient
k_B	Back emf constant of the macro actuator
k_b	Back emf constant of the micro actuator
k_d	Differential gain
k_G	Gear ratio of the macro actuator
k_g	Gear ratio of the micro actuator
k_I	Torque constant of the macro actuator
k_i	Torque constant of the micro actuator
k_p	Proportional gain
l	Link length
L_M	Inductance of the macro actuator

L_m	Inductance of the micro actuator
L_{c-i}	Center of mass of L_i
M	Mass inertia matrix
m	Mass of the end-effector
m_a	Mass of the lead nut
M_i	Mass of the link L_i
$M_{actuator}$	A diagonal inertia matrix containing all actuator and gearbox inertia
N	Number of (-1,0) clockwise encirclement
n	Pitch of the lead screw per radian
P	Number of poles of loop gain in RHP
p	Pitch of the lead screw
$P(t)$	Estimator gain matrix
q	Output signal
q_j	Vector of generalized coordinates
r	Link length
R_i	Rotation matrices
R_M	Resistance of the macro actuator
R_M	Resistor of the macro actuator
R_m	Resistance of the micro actuator
R_m	Resistor of the micro actuator
s	Sliding variable
T	Kinetic energy
T_L	Load torque of the macro actuator
T_i	Load torque of the micro actuator
T_M	Motor torque of the macro actuator
T_m	Motor torque of the micro actuator
V	Control input
V	Potential energy
V_B	Back emf Voltage of the macro actuator
V_b	Back emf Voltage of the micro actuator
V_M	Voltage of the macro actuator
V_m	Voltage of the micro actuator
$W(q, \dot{q})$	Filtered regressor matrix
$w(t)$	Input control vector of the feedback linearization method
X_i	Cartesian coordinate of the link i
Z	Number of zeros of sensitivity function in RHP
ϵ_f	Filtered prediction error
ω	Gain of low pass filter
τ	Torque applied to the rotation joint φ
τ	Torque of an actuator

\tilde{C}	Modeling error of the vector of Coriolis and centrifugal torques
\tilde{G}	Modeling error of the vector of gravitational torques
\tilde{M}	Modeling error of mass inertia matrix
F	Force applied to the translation joint a
L_i	Links of the Delft robot arm
q_d	Desired output signal
q_r	One of control inputs in the sliding mode algorithm
T_j	Jacobian matrix of global coordinates
V_f	Filtered control input
y	Filtered control input ($=V_f$)
g	Gravity constant